AD-A144 334 AMPLITUDE/PHASE MONOPULSE RECEIVER COMPARISON(U) 1/1
FEDERAL AVIATION ADMINISTRATION TECHNICAL CENTER
ATLANTIC CITY NJ R J ALIMENTI ET AL. JUL 82
UNCLASSIFIED FAA-CT-82-100-82LR F/G 17/3 NL

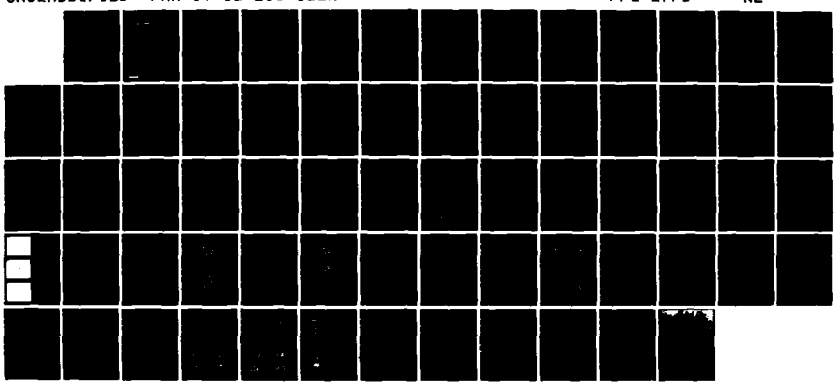

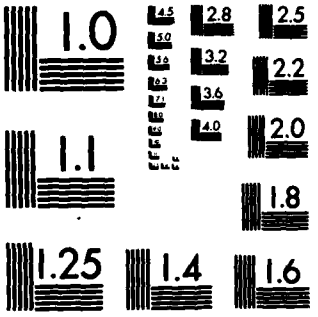

MICROCOPY RESOLUTION TEST CHART
NATIONAL BUREAU OF STANDARDS-1963-A

FAA TECHNICAL CENTER LETTER REPORT

AMPLITUDE/PHASE MONOPULSE RECEIVER COMPARISION

by

RAYMOND J ALIMENTI
DANIEL P FOX
JOHN KENTON

JULY 1982

U. S. DEPARTMENT OF TRANSPORTATION
FEDERAL AVIATION ADMINISTRATION
TECHNICAL CENTER
Atlantic City Airport, N.J. 08405

TABLE OF CONTENTS

Title	Page
INTRODUCTION	1
Purpose	1
Background	1
DISCUSSION	2
Description of Equipment	2
Test Approach	8
Data Collection	11
Data Reduction	25
RESULTS AND ANALYSIS	26
Static Tests	26
Ground Accuracy Tests	33
Flight Tests	47
Interference Tests	49
SUMMARY OF RESULTS	58
CONCLUSIONS	59
REFERENCES	60

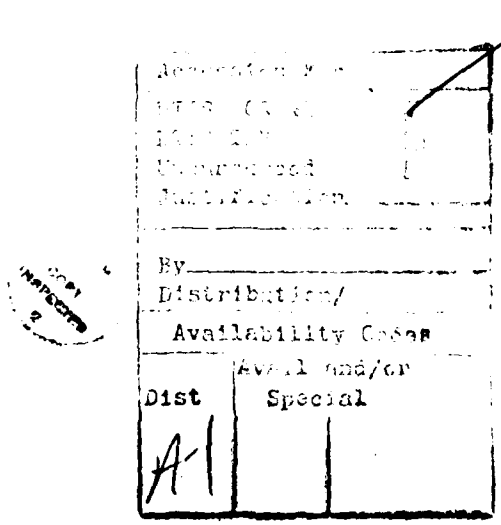

LIST OF FIGURES

Figure		Page
1	Phase Monopulse Receiver	4
2	Amplitude Monopulse Receiver	5
3A	Monopulse Response: Amplitude Receiver	6
3B	Monopulse Response: Phase Receiver	7
4	CW Static Test Setup	12
5	Pulsed Static Test Setup	14
6	Receiver Tracking Setup	16
7	Receiver Sensitivity Setup	17
8	Distribution of GA Transponder Frequencies	19
9	Interference Test Setup	22
10A	Receiver Response: Log Output vs. Input Power	27
10B	Receiver Response: Log {D}-Log {S}	28
11	Receiver Response: Delta/Sum Ratio Output vs. Sum Input	29
12	Amplitude Receiver Response: Monopulse Video vs. Input Power	30
13	Receiver Bandwidth: Delta/Sum vs. Frequency	31
14A	Receiver Bandpass: Log Output vs. Frequency	32
14B	Delta minus Sum Log mplifier Bandpass	34
15	Receiver Tracking: Delta/Sum Output vs. Delta/Sum Ratio	35
16	Log Amplifier Tracking Photographs	36
17	Receiver Sensitivity: Bracket Detects/Sec vs. Input Power	37
18A	Amplitude Receiver Azimuth Accuracy	39
18B	Amplitude Receiver Monopulse Curve	40
18C	Phase Receiver Azimuth Accuracy	41
18D	Phase Receiver Monopulse Curve	42
19A	Phase Receiver Off-frequency Error Data	43

LIST OF FIGURES (con't)

Figure		Page
19B	Amplitude Receiver Off-Frequency Error Data	44
20	Phase Receiver Low Power Error	45
21	Amplitude Receiver Low Power Error	46
22	Amplitude Receiver Power Variation Error	48
23	Phase Receiver Flight Test Azimuth Residual Histograms	51
24	Amp Receiver Flight Test Azimuth Residual Histograms	52
25	Interference Effects: No Inteference and 100 Mode S, SIR=-10 dB	53
26	Interference Effects: 5K and 16K ATCRBS, SIR=-10 dB	54
27	Interference Effects: 16K ATCRBS, SIR=-20 dB	55

LIST OF TABLES

Table		Page
1	Basic (CW RF) Static Test Variables	13
2	Flight Plan for Phase/Amplitude Monopulse Comparison	21
3	Interference Correction Table	24
4	Flight Test Results (AU's)	50
5	Mode S Replies/Scan Under Interference	57

INTRODUCTION

PURPOSE

The purpose of this test effort was to collect performance data on a phase and an amplitude type monopulse receiver that would provide a basis for comparing the relative tradeoffs of the two approaches. In particular, the thrust of this effort was to evaluate the azimuthal accuracies and the useable beamwidths of each type of receiver. It is expected that the results of the testing conducted under this effort will form part of the basis for assessing the merits of either approach if proposed for the production Mode S sensors.

BACKGROUND

The Federal Aviation Administration (FAA) has, since 1979, been engaged in the test and evaluation of three Mode S sensors built by Texas Instruments (TI), Inc. Constructed in accordance with specifications contained in the engineering requirement, FAA-ER-240-26 (Reference 1), these sensors provide an angular tracking accuracy for Air Traffic Control Radar Beacon System (ATCRBS) and Mode S transponder equipped aircraft of 0.1 degree root mean squared (rms). This accuracy has been attained, in part, through the incorporation of a sum and difference monopulse receiver for estimating off boresight angles.

The receiver design implimented in the Mode S sensors is a phase-type known as a half angle processor (reference 2). In this approach the received difference ({D}) and sum ({S}) levels are converted to phase information at the radiofrequency (RF) level. The relative intermediate frequency (IF) phase values of the {D} and {S} channels are then combined to estimate ABS[{D}/{S}], i.e., the monopulse value. Although this approach has fulfilled the angular accuracy requirements (reference 3) specified in the ER, alternate receiver designs are possible which may fulfill the Mode S accuracy requirements and, at the the same time, provide certain advantages in terms of cost, complexity, and the level of maintenance skills required by service personnel. One candidate approach, known as an amplitude monopulse receiver, has been specifically cited as having these very qualities, and, therefore, worthy of comparison with the phase receiver in tne Mode S sensor. Basically, an amplitude monopulse receiver functions by generating the {D}/{S} ratio directly from the IF {D} and {S} signal amplitudes, normally after logarithmic amplification.

Since both approaches are likely to be proposed for the "front-end" of the FAA's production Mode S sensor, it was decided that a test effort was required to provide comparative data for evaluating the relative performance tradeoffs of each approach. In order to accomplish this testing, the FAA's Technical Center designed and installed a modification into the Mode S sensor located at the Center that would convert the front-end to an amplitude processor.

This document describes the testing performed on each receiver and the results of those tests. Also included is a description of the circuitry used to modify the Mode S sensor to operate in an amplitude mode.

DISCUSSION

DESCRIPTION OF EQUIPMENT

MONOPULSE RECEIVERS. The Mode S receiver is a three channel system that operates on sum, difference, and control (Omni {O}) RF inputs. The sum and difference signals are derived from a 5-foot open array antenna, while the control signal is derived from the omnidirectional antenna of the sensor. The control signal is used for the suppression of replies that occur in the side-lobes of the directional antenna, i.e., it provides for receiver side-lobe suppression (RSLS). The sum and difference signals provide information necessary to make off-boresight estimates. Development of the sum and difference signals is performed via a hybrid junction, which adds and subtracts vectorially the signals from the right and left halves of the antenna. Due to the linear combination of the two halves of the antenna, the sum and difference signals are either in phase or 180 degrees out of phase with respect to each other. The state of the relative phase is a function of whether the received signals originate from a target that is to the right or to the left of the antenna's electrical center plane, i.e., the antenna's boresight.

In the amplitude system, the individual sum and difference signals are logarithmically amplified and combined to form a function of the {D}/{S} ratio, e.g. Log({D}/{S}), as an estimator of the off-boresight angle of the target.

In the phase monopulse receiver the individual sum and difference signals are combined in a hybrid junction to form two intermediate vectors i.e., {S}+j{D} and {D}+j{S}, which approximates the situation of two overlapping antennas with displaced phase centers. The two signals, normally referred to as the A and B vectors, have the characteristic that the angle between them provides an estimator, which is related to the amplitudes of the {S} and {D} antenna patterns and, therefore, the monopulse function.

As noted in reference 2, the monopulse function can be approximated near boresight by a phase detector having a sine output, i.e.,

$$\text{Monopulse function} = (\sin \{P\})/2$$

where {P} is the angle between the A and B vectors.

An ambiguity arises, however, when abs({D}/{S})>1. This occurs when {P}>90 degrees. Therefore, the {D}/{S} antenna crossover points mark the limits of the usable range of the off-boresight estimator. To extend the range of the angle estimator, a half-angle approach has been used in the Mode S receiver. In this approach, the angle between the A and B vectors is divided to form secondary vectors whose angles are always less than 90 degrees. The two angles are defined as follows (reference 2):

$$\{a\}, \{b\} = \arg(\{S\} +/- j\{D\}) - \arg(\{S\})$$

This process results in two angles that can be phase detected individually and unambiguously. The outputs of the phase detectors are then combined linearly to form {P}, since (reference 2):

$$\{P\} = a - b$$

RECEIVER MODIFICATION. The implementation of the half-angle processor used in the Mode S sensor is shown in figure 1. The modifications used to convert this receiver into an amplitude receiver are shown in figure 2. The major differences between the two occur in the retention of the original {D} and {S} signals in the amplitude system with the removal of the 90 degree hybrid. The second major difference occurs with the replacement of the IF hybrids (the heart of the half-angle processor) with a subtractor circuit to form log (abs({D}/{S})) in the amplitude processor.

It will also be noticed in figure 2 that two amplifiers, one inverting and the other noninverting, follow the subtractor circuit. This was done for two reasons: (1) the subtraction of the {S} and {D} signals results in an output that is symetrical with respect to boresight, i.e., the sense or relative phasing of the {S} and {D} signals is not present; and (2) in order for the circuit to be compatible with the A/D converter used in the Mode S sensor bipolar video had to be used, positive for right and negative for left of boresight. To fulfill these requirements the two amplifiers provide mirror image curves, one positive and one negative, to an analog multiplexer. The particular curve is then chosen on the sense of the {D} and {S} signals.

In order to detect the sense of the sum and difference signals, each are seperately amplified, limited, and, subsequently, fed into a balanced mixer acting in a phase detector mode. The output of the mixer is then used to control the multiplexer and to select the appropriate video for the A/D converter.

A consequence of the design used was that a linear subtraction of the delta from the sum resulted in problems near boresight due to antenna characteristics. That is, the delta/sum ratio near boresight varies as a function of elevation angle and can be between 29 to 36 dB. The prexisting circuitry which the amplitude modification was to function with, required all monopulse video right of boresight to be positive and all left of boresight to be negative. A clipping circuit was, therefore, employed to maintain a consistant voltage for all null depths which could be encountered near boresight. This modification also made the amplitude circuit's response very similar to that of the phase receiver, as can be seen in figures 3a an 3b.

MODE S SENSOR OPERATION. Two factors that affect the azimuth reporting accuracy of the Mode-s sensor are the means by which it is calibrated and the different interrogation schemes used for Mode S and ATCRBS aircraft.

In order for the Mode S sensor to determine accurately the azimuth of a transponder equipped aircraft, it must provide a means for translating the {D}/{S} ratio into a measure of the target's distance from boresight or off-boresight angle. This is accomplished via a stored calibration table that relates a given monopulse number, i.e., {D}/{S} ratio, with an off-boresight correction that is added to the pointing angle of the sensor's antenna. The correction table itself is generated by interrogating a fixed transponder with a known position over many antenna scans. Once sufficient data points have been recorded, a smoothing process is applied to the table which results in a single off-boresight correction for each monopulse value. The final corrections are often referred to as the monopulse curve or table, terms that will recur in this report.

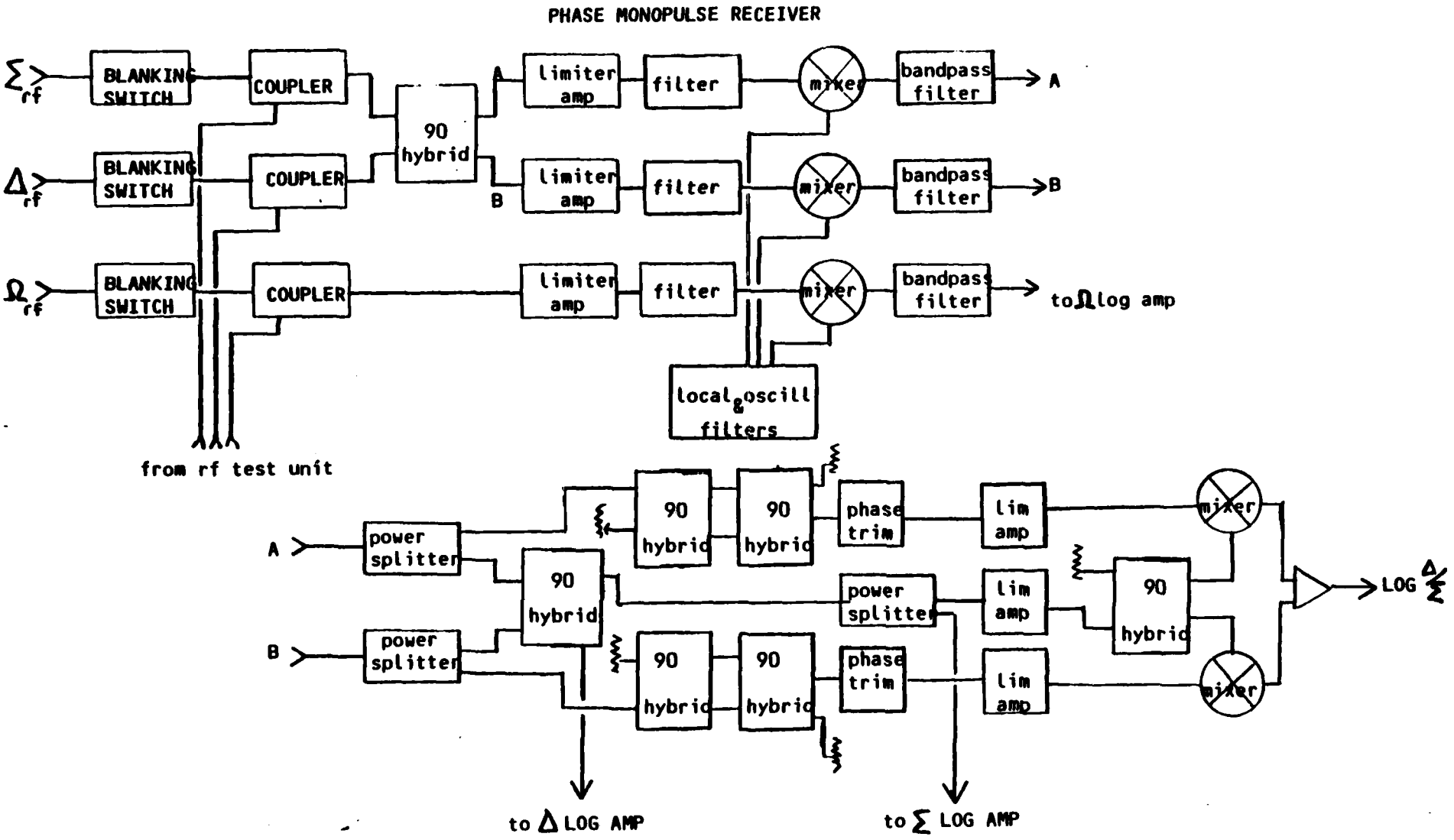
PHASE MONOPULSE RECEIVER
BLANKING SWITCH
COUPLER
90 hybrid
limiter amp
filter
mixer
bandpass filter
A
B
to Ω log amp
local oscill filters
from rf test unit
power splitter
phase trim
lim amp
LOG
to Δ LOG AMP
to Σ LOG AMP

FIGURE 1

AMPLITUDE MONOPULSE RECEIVER

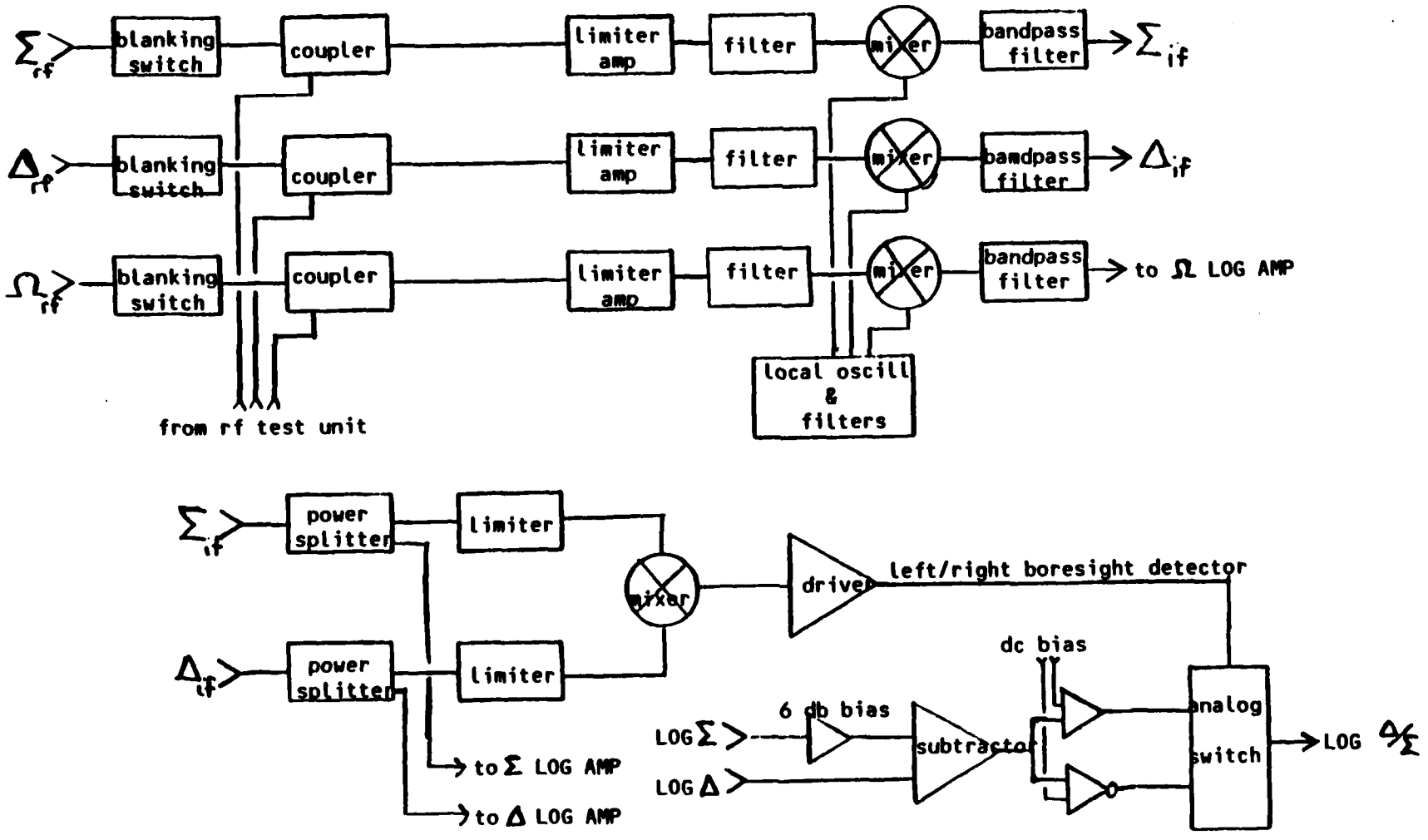

FIGURE 2

X RANGE, Y RANGE = -35 6 -2.81 3.288
SELECT OUTPUT
1-SUMOUT, 2-DELOUT, 3-DEL/SUMOUT, 4-MONOUT, 5-NO PLOTS

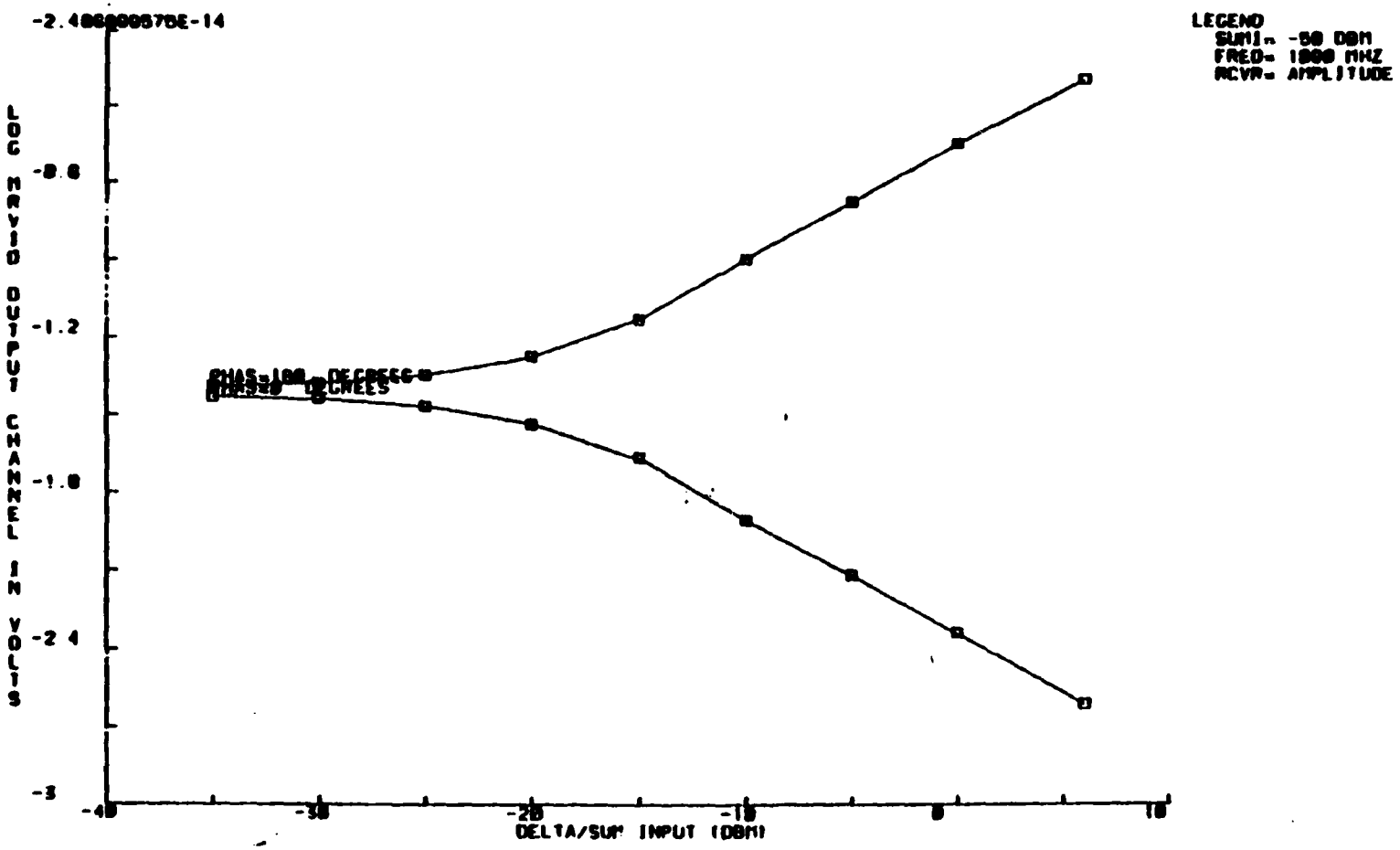

FIGURE 3A. LOC MRVID OUTPUT CHANNEL VS INPUT D/S RATIO & PHASE

X RANGE,Y RANGE = -35 0 -2.79 3.885
SELECT OUTPUT
1-SUMOUT,2-DELOUT,3-DEL/SUMOUT,4-MONOUT,5-NO PLOTS

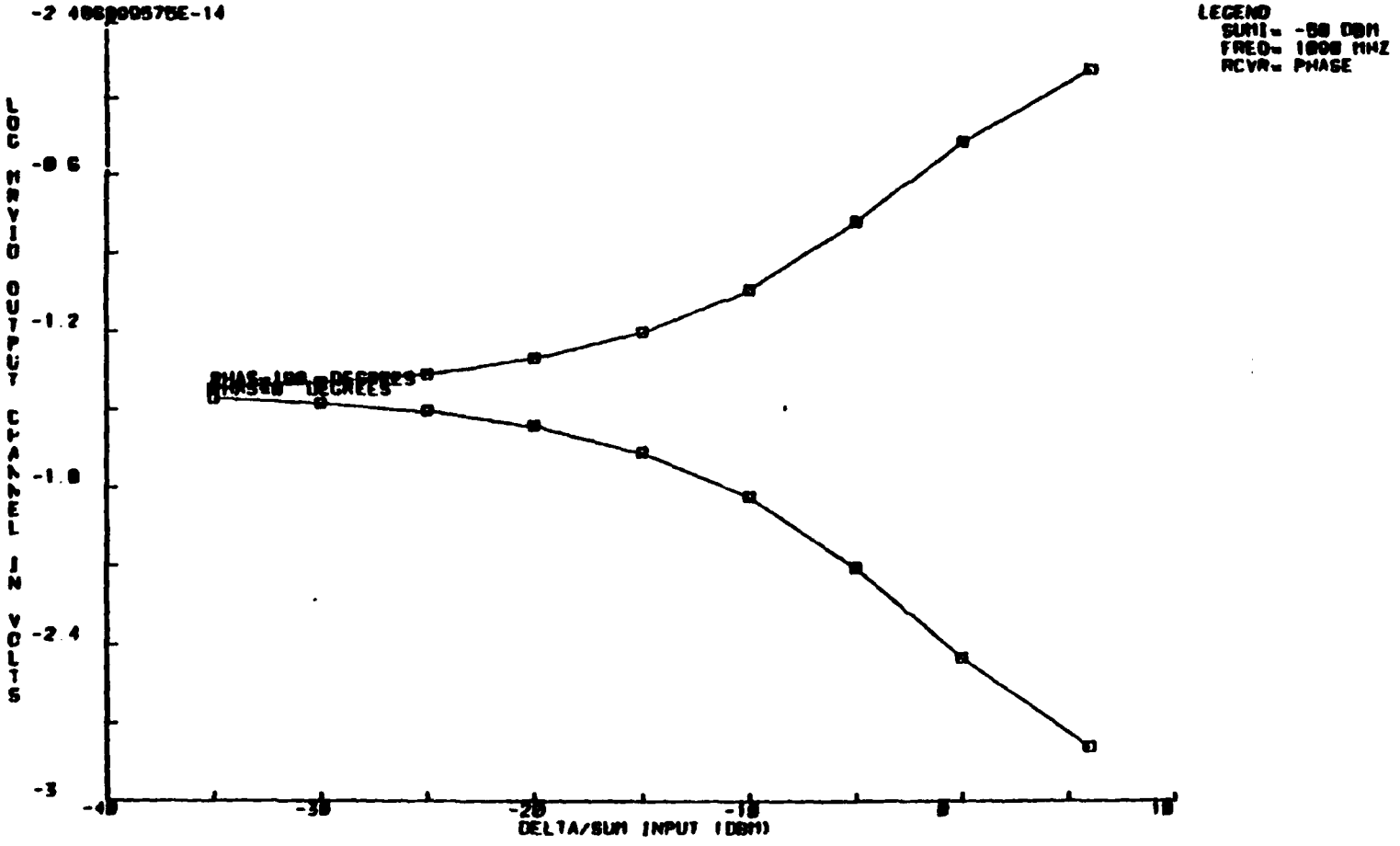

FIGURE 3B LOG MRVID OUTPUT CHANNEL VS INPUT D/S RATIO & PHASE

To assure the greatest accuracy in establishing the monopulse table, the location of the fixed transponder (known as the Calibration and Performance Monitoring Equipment (CPME)), with respect to the sensor, was surveyed at the time of installation and is known to be within +/-0.0028 degrees in azimuth and +/-5 feet in range. This degree of survey is documented in reference 2 as a Second Order, Class II Survey as defined by the Federal Geodetic Control Committee.

The Mode S sensor has essentially two modes of interrogation, depending on whether the sensor is in an ATCRBS or Mode S interrogation cycle (scheduling of these cycles is performed by the sensor's Channel Management function). Interrogation of ATCRBS targets occurs at regular fixed intervals in much the same way as current ATCRBS interrogators. This means that the resulting replies cover the beamwidth of the sensor's antenna. The azimuth used by the sensor in the ATCRBS target report for each scan is formed by averaging the replies that are closest to boresight. The net effect is that the ATCRBS reports give preference to replies closest to the boresight of the antenna and are, therefore, subject to the accuracy and stability of the monopulse function at boresight. The scheduling of Mode S interrogations however, is performed in a fashion that will maximize the amount of antenna dwell time on the target. In order to accomplish this, the scheduling algorithm for discrete interrogation is designed to "catch" targets as close to the leading edge of the antenna beam as possible. This approach results in the predominant number of Mode S replies occurring in areas of the antenna pattern beyond the sum and difference crossover points. It is, therefore, significant that any monopulse receiver design for Mode S must operate throughout the entire beamwidth of the antenna including areas beyond the sum and difference crossover.

TEST APPROACH

The testing performed in this program was divided into four phases: Static Tests, Ground Accuracy Tests, Flight Tests, and Interference Tests. The purposes and the general approach to each are described in the following paragraphs. Also, see the test plan, CT-82-100-10LR (reference 4) and the addendum to CT-82-100-10LR (reference 5). The specifics of the tests involved and the conduct of the individual tests are presented in the "Data Collection" section of this report.

The overall approach to this program was to conduct all testing on the phase and amplitude receiver within the environment of the same sensor, i.e., to keep all hardware elements the same except for those required to effect a changeover from a phase to an amplitude receiver and back. In this way all elements, except for those identified in the "Receiver Modification" section were the same throughout the testing.

STATIC TESTS. The static tests were designed to establish the response and tracking characteristics of the sum (S) and difference (D) channels of each receiver. Additionally, tests were performed to determine the detection characteristics of the receivers to simulated ATCRBS targets. Receiver response and tracking were determined by injecting CW RF signals of varying frequencies, signal strengths, and (D)/(S) ratios

into the {S} and {D} channels of each receiver. The range of frequencies used covered the 1090 +/-3 MHz band, while the sum signal strength varied over the dynamic range of the receivers, i.e., -20 to -79 dBm referenced to the sensor's RF port. (This report will follow tne convention of defining the RF port as the output of the antenna's rotary joint.) The {D}/{S} ratios ranged from -30 dB (boresight) to +6 dB, i.e., an area beyond the crossover points of the sum and difference antenna patterns. Receiver detection for both receivers was performed at 1090 MHz.

GROUND ACCURACY TESTS. Tests were performed with each receiver in order to determine the sensor's accuracy with respect to a fixed geodetic point. For this testing the CPME of the subject sensor was utilized.

At the same time that this testing was being performed, off frequency and low power tests were performed by varying the response frequency and transmit power of the CPME. The range of frequencies and power levels used varied over 1090 +/- 6 MHz and from -50 to -79 dBm referenced to the sensor's RF port.

FLIGHT TESTS. Flight tests were performed in order to compare the target report accuracy of the Mode S sensor when operating with the amplitude or the phase receiver. This was done with an aircraft equipped with an ATCRBS and a Mode S transponder and employed the use of the Technical Center's Nike tracking radar as an overall reference.

In order to minimize errors in the position determination of the tracking radar, the flight profiles were limited to a series of radial runs along a line joining the sensor and the tracking radar. The flights were performed at three altitudes and extended from 6 to 40 nautical miles (nmi).

The data collected was used to determine the differences, i.e. residuals, between the angular determinations of the tracking radar and the Mode S sensor. The residuals were used to constitute an estimator for angular accuracy. In these tests the tracker was regarded as the reference.

INTERFERENCE. Tests were performed to identify the extent to which ATCRBS and Mode S fruit, i.e., nonsynchronous replies, affect the azimuthal accuracy and variance of the phase and amplitude receivers. These tests were performed in terms of the relative signal-to-interference ratio (SIR), angular seperation between the interference and a fixed target, and fruit rates. To accomplish this, simulated ATCRBS and Mode S fruit were injected into the sensor at the RF level while the sensor interrogated the CPME. The SIR's employed were -10, 0, and +10 dB, although several tests were conducted at +20 and -20 dB SIR. The fruit rates covered were 50 to 200 Mode S fruit/sec while ATCRBS fruit ranged from 1.7K to 16K fruit/sec. Angular seperations between the source of the fruit and target replies covered the entire beam of the antenna. This was accomplished by establishing a fixed {D}/{S} ratio for the fruit while scanning the target (the CPME). The {D}/{S} ratios were set to establish the source of the interference as originating at boresight, at the {S} and {D} crossover points, and at a point beyond crossover (the +6 dB point).

In the performance of the interference tests the definition adhered to for SIR was the ratio of the received signal strength, as measured at output of the sum channel, of the target, i.e., the CPME, to that of the fruit when both were at boresight. This meant that any fruit originating at points in the antenna beam other than boresight would be reduced accordingly to reflect the antenna's amplitude pattern.

Only the results of the effects of fruit on Mode S replies are shown in this report. The fruit effects on ATCRBS replies will be presented at a later date, as an addendum to this report.

DATA COLLECTION

The testing series that was performed during each phase of this program is presented in the following paragraphs. The types of data collected and the methodology for collecting that data are presented.

STATIC TESTS. The static tests were divided into three categories based on the functional intent of each test. These categories include determining: (1) the overall response of each type of receiver, (2) the tracking of the individual channels of each receiver, and (3) the detection characteristics of each receiver as a function of received signal strength.

Two test configurations were used during the static tests. In one case shown in figure 4, a continuous wave (CW) RF signal was injected into the {S} and {D} ports of the sensor. The relative magnitudes of each signal were varied in order to establish the {S} signal at the desired level referenced to the sensor's RF port, while the {D} signal was set to the appropriate {D}/{S} ratio. This test configuration was used initially to gather data on the response of each receiver to a broad range of input variables. The range of input variables and the output measures recorded are listed in table 1.

For certain tests it was necessary to modify the configuration in figure 4 to accomodate a pulsed RF signal. The second test setup is shown in figure 5. In this configuration a PIN diode modulator was driven by either the sensor's Test Target Generator (TTG) or, in certain cases, a pulse genrator. (The TTG is a piece of test equipment supplied with the sensor and provides the capability of providing both ATCRBS or Mode S type replies, as well as all interfacing to the transmitter control functions of the sensor.) The {D}/{S} ratios were established in the same fashion as in the CW test configuration.

RECEIVER RESPONSE. Data for these tests were derived from the basic static test configuration using CW RF. Two additional tests were performed using pulsed RF signals. In the first it was desired to determine the amplitude response of the Log {S} and Log {D} amplifiers. This was done on the receiver configured for an amplitude system. In this way each of the two log amplifiers were at the end of two relatively isolated RF/IF channels. The tests were conducted by varying the input signal from -20 to -85 dBm in 1 dB increments. This was accomplished by inserting a calibrated step attenuator before the power divider in figure 5, and recording the ouput peak voltage of the two Log amps using a high gain differential amplifier. Throughout these measurements, the {D}/{S} ratio was kept at 0 dB.

The other additional test performed for receiver response was to record the output voltage of the Monopulse Receive Video (MRMVD) over the full dynamic range of each receiver. The MRMVD was selected for measurement because it is the input to the A/D converter where the monopulse value is established. This test was conducted using the same setup as used for the amplitude response of the log amplifiers. The only difference was in terms of the input powers used. The input was varied from -15 to -90 dBm in 5 dB increments, and then from -90 to -112 dBm in 1 dB increments. As in the log amplifier measurements, the {D}/{S} ratio was 0 dB.

CW STATIC TEST SETUP

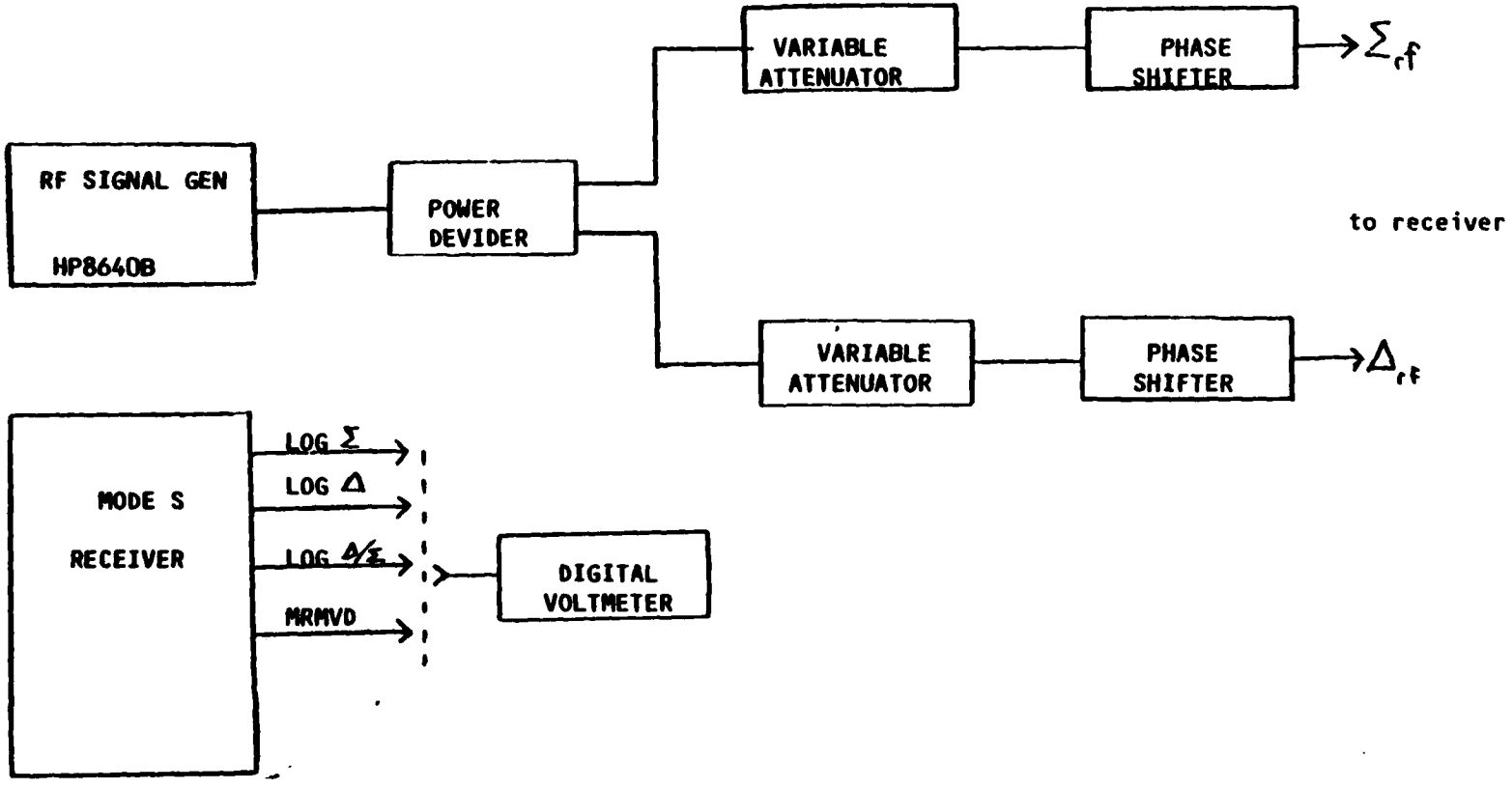

FIGURE 4

TABLE 1 BASIC (CW RF) STATIC TEST VARIABLES

INPUTS

Sum power (dbm): -25, -30, -40, -50, -60, -70, -80
Delta/Sum (db): +6, 0, -5, -10, -15, -20, -25, -30, -35
Frequency (MHZ): 1087, 1088, 1090, 1092, 1093,
Delta/Sum relative
phase (degrees) : 0, 180

OUTPUTS

Log Sum, Log Delta, Delta/Sum, MRMVD

Notes:
1. The MRMVD is the input to the A/D converter. It is essentially the amplified Delta/Sum signal
2. In the case of the amplitude receiver the Delta/Sum signal is the output of the implimented subtractor circuit and is therefore the Log(Delta/Sum)

PULSED STATIC TEST SETUP

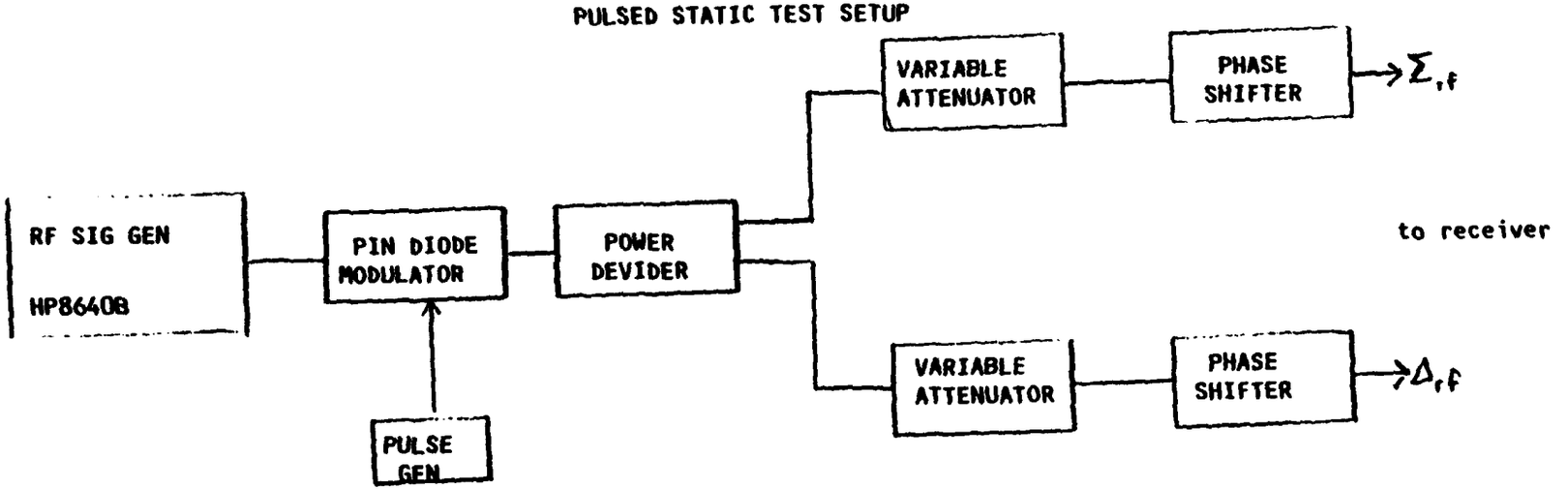

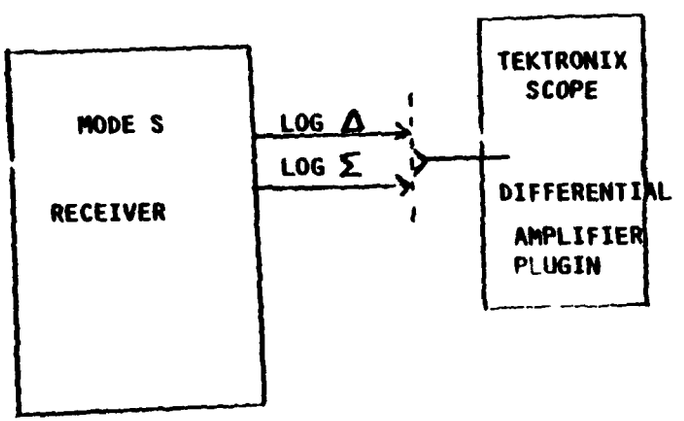

FIGURE 5

RECEIVER BANDWIDTH. Most of the data for determining the bandwidth of each receiver originated with the basic CW test. An additional set of measurements were made using pulsed RF. These were made with the {D}/{S} ratio at 0, dB while the effective input power to each channel was set at each of five different levels: -25, -35, -50, -65, and -80 dBm. At each power setting the input frequency was varied from 1085 to 1095 MHz in 1 MHz increments. The resulting peak voltages of the log{S} and log{D} amplifiers were then recorded. For the same reason of isolating the two RF/IF channels mentioned in the "Receiver Response" section, these measurements were performed only on the amplitude system.

RECEIVER TRACKING. As in the foregoing sections, data for receiver tracking were derived in part from the basic CW tests. Because of the need for precise tracking between the log amplifiers in an amplitude monopulse receiver, it was decided to gather data that would aid in interpreting the overall tracking of the two. This was done by using the basic CW test configuration and modifying it to include an 80 dB voltage controlled attenuator (VCA) before the power divider (figure 6). Since the VCA provides a logarithmic function using a segmented approximation technique, although with many more stages than the log amplifiers in the sensor, the log{D} or log{S} output should be a linear function of the control voltage for the VCA. There are, of course, certain limitations to this, primarily the relative response times of the VCA and the log amplifiers. In order to minimize these possible effects, the control voltage of the VCA was established as a sawtooth (increasing attenuation) over a period of 10 mS, with a repetition rate of approximately 11 to 12 mS. The outputs of the log{S} and log{D} were then subtracted using the high gain amplifier mentioned previously. The resulting signal, along with the {D}/{S} output of the sensor (log{D}/{S}), were then photographed on an oscilliscope.

RECEIVER DETECTION. As a final static baseline for comparison of the two receivers, as well as to determine their respective sensitivities, data were collected on the number of bracket detections that occur for injected ATCRBS replies. This was done by using the pulsed RF setup with the driving signal for the modulator coming from the TTG test set (see figure 7). The input frequency was 1090 MHz, while the {D}/{S} ratio was maintained at 0 dB. The input power was varied from -74 to -85 dBm (referenced to the RF port) in 1 dB increments. The number of injected ATCRBS replies was 3906/sec (a number that was controlled by the interface logic between the sensor and the TTG). The number of bracket detects was measured by using a counter to monitor the bracket detect signal in the sensor's ATCRBS processor. This process was repeated for both receivers. (The 90 percent bracket detect point for the sensor is specified to occur at -79 dBm (reference 1)). Throughout the testing no signals were injected throught the omni RF port. During the tests the thresholds of the video digitizer were left at their nominal settings:

Threshold	Setting
TSA (Fixed Sum ATCRBS)	-82 dBm
TSTCA (ATCRBS Sensitivity Time Control)	OFF

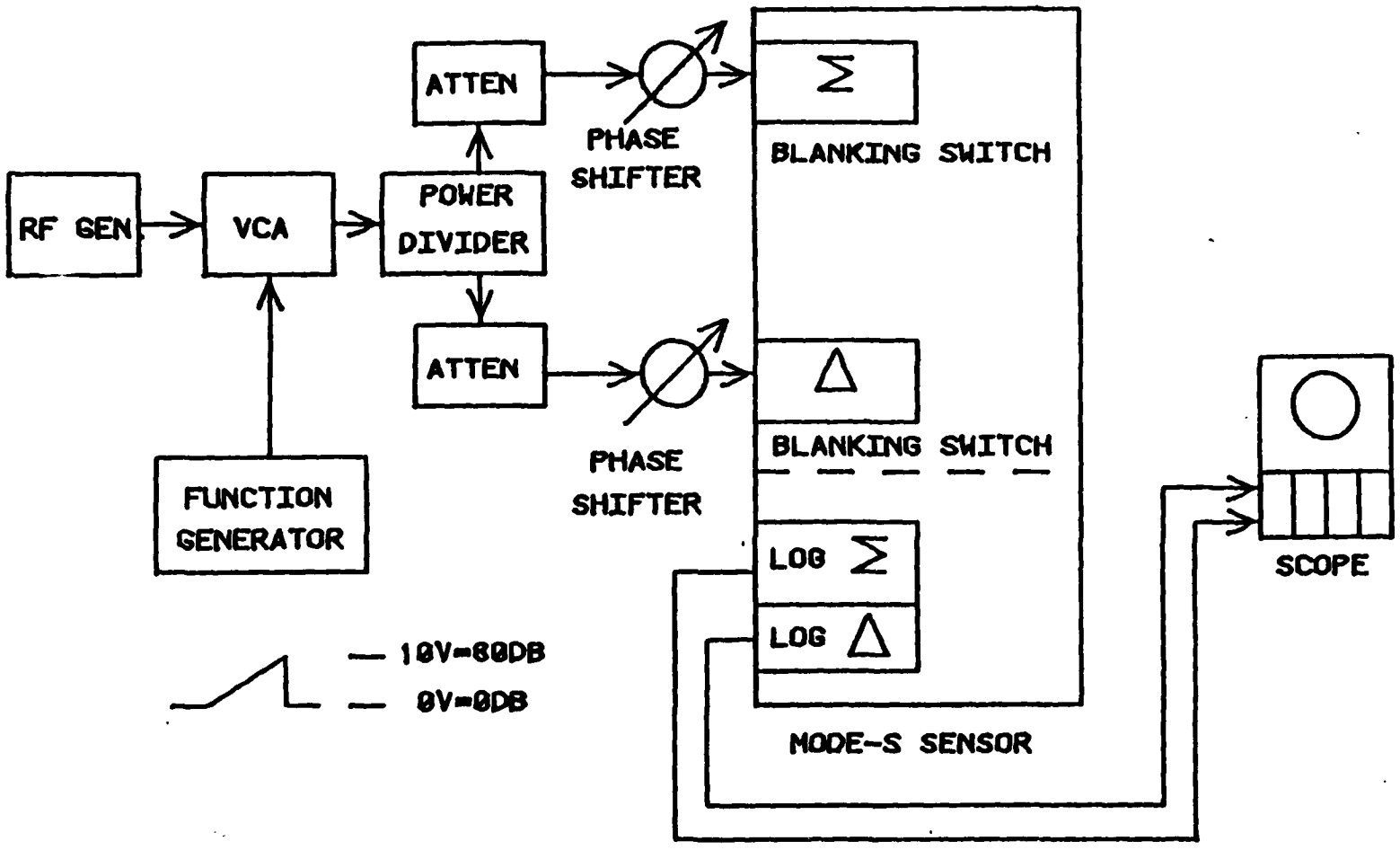

FIGURE 6 TEST CONFIGURATION FOR LOG AMPLIFIER TRACKING

RECEIVER SENSITIVITY SETUP

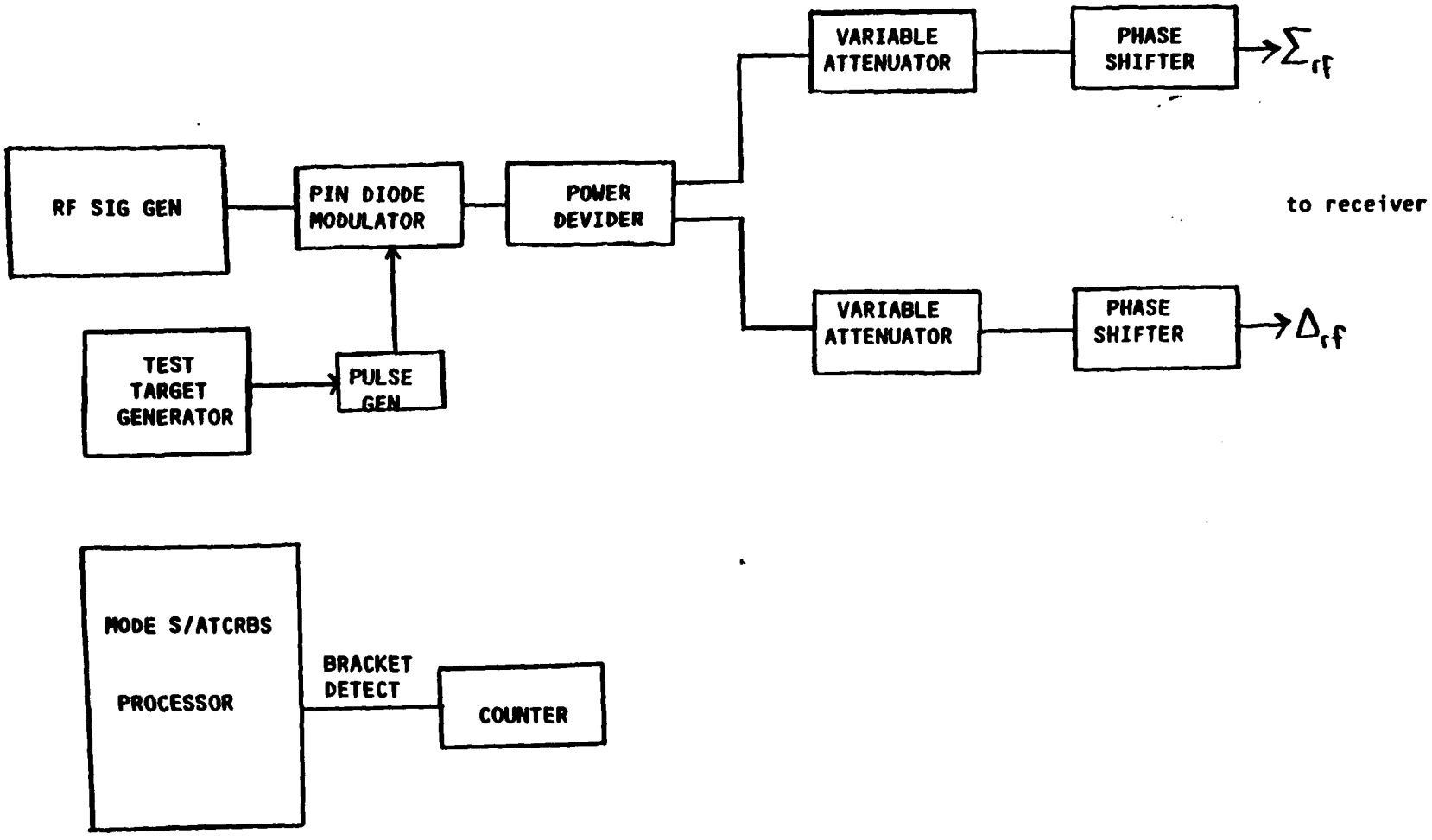

FIGURE 7

GROUND ACCURACY TESTS. The ground accuracy tests were divided into two stages based on their functional objectives: (1) establishment of the azimuth errors due to off-frequency replies, and (2) to establish the effects of low received power levels. In each case, the sensor's CPME was the source of target replies. During off-frequency testing the RF source for the CPME was replaced by a calibrated RF signal generator .

Throughout these tests the primary form of data collection was via the sensor's Range and Azimuth Accuracy diagnostic (RAA). Essentially, RAA functions by scheduling a high number of interrogations of the CPME for the period of time that the sensor's antenna beam is scanning the CPME. The resulting monopulse value, i.e., the measured {D}/{S} quantity for each increment in azimuth, is then used by the sensor to derive off-boresight azimuths of the CPME in azimuth units (AU's) fron the mono-pulse lookup table. The RAA diagnostic then calculates the difference between the calculated bearings of the CPME based on the monopulse table and the known location of the CPME. (The location of the CPME is an opera-tor input paramater to the RAA diagnostic.) This process results in a series of differences in AU's between the measured CPME location based on the monopulse value and the surveyed location of the CPME for each change in antenna pointing angle. The range of angles normally processed by the RAA extends beyond the 3 dB beamwidth of the antenna.

AZIMUTH ACCURACY. In this test the CPME reply frequency was established at 109(MHz. The RAA diagnostic was used to establish the azimuth accuracy of the sensor.

OFF FREQUENCY. The data collection process followed in the foregoing sectio. was repeated with the CPME operating at 1086, 1087, 1088, 1092, 1093, and 109(MHz. The reply frequency of the CPME was established by using a stable external RF signal generator in place of the CPME's normal local oscillator. Throughtout the tests the frequency of the generator was monitored at the CPME to assure minimal variations.

The selection of frequencies was extended 1 MHz beyond the normal +/- 3 MHz tollerance of transponders. This was done to assure coverage of as much of the frequency spread of general aviation (GA) transponders as possible. Data summarizing the distribution of GA transponder frequencies as measured between the years of 1977 and 1980 has been excerpted from references 6 to 8 and is presented in figure 8.

LOW POWER. In order to assess the impact upon the azimuth accuracy determi-nations due to reduced signal levels, the CPME output power was reduced to levels between -70 and -79 dBm. System calibration for the low power tests was done at a received power level of -54 dBm. The power was then reduced to each of the desired power levels at the CPME by means of a step attenuator. Data were collected at -70, -74, -76, -77, -78, and -79 dBm using the RAA program. All tests were done at a frequency of 1090 MHz.

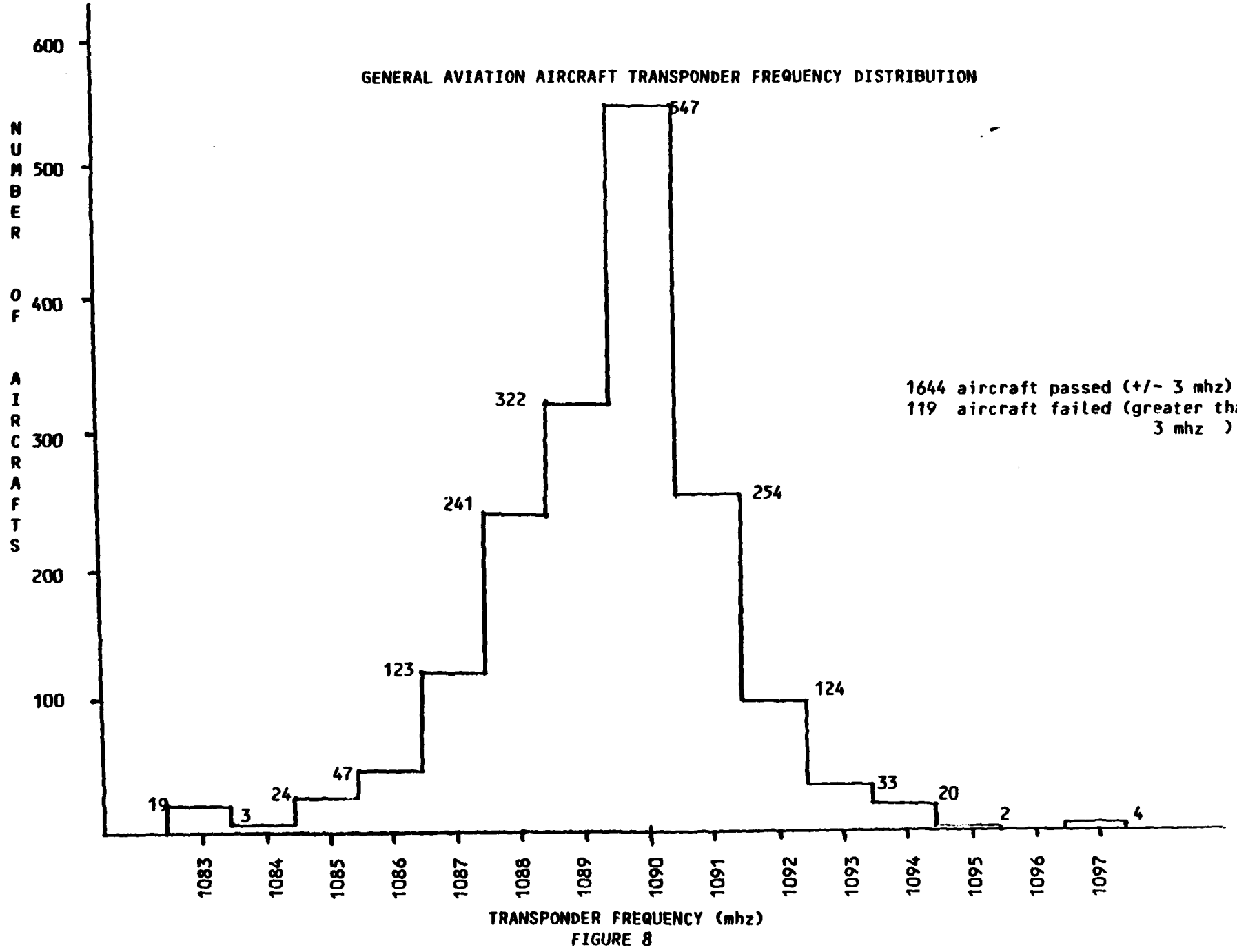
GENERAL AVIATION AIRCRAFT TRANSPONDER FREQUENCY DISTRIBUTION
NUMBER OF AIRCRAFTS
600
500
400
300
200
100
547
322
241
254
123
124
47
33
24
20
19
3
2
4
1644 aircraft passed (+/- 3 mhz)
119 aircraft failed (greater than 3 mhz)
1083
1084
1085
1086
1087
1088
1089
1090
1091
1092
1093
1094
1095
1096
1097
TRANSPONDER FREQUENCY (mhz)

FIGURE 8

FLIGHT TESTS. The flight tests were conducted using the Technical Center's Nike tracking system. In order to assure an uninterrupted source of tracking data, both the target tracking radar (TTR) and the missle tracking radar (MTR) of the Nike system were used.

The flights were performed with the unmodified Mode S phase monopulse receiver during 1 day of flying. A second flight date was reserved to repeat the same flights with the modified Mode S amplitude receiver.

The flight plan for the tests was composed of three radial flights, each of which was made up of one inbound and one outbound run (see table 2). Each radial flight was performed along the same radial at three different altitudes. The radials were selected along a line of maximum accuracy for the Nike tracking radar. Orbital flights were originally planned for inclusion in these tests, but were cancelled for two reasons. The first was due to airspace restrictions, and the second was that orbital flights would contribute little more to assessing azimuth accuracy than would the radial flights.

In order to minimize flight time and to permit data collection for both an ATCRBS and a Mode S target simultaneously, the aircraft was equipped with two seperate transponders, one ATCRBS and one Mode S TRU-2 transponder. Both were active at the same time during the flights. Prior to the flights, each transponder was checked to ascertain the center frequency of their transmissions, i.e., 1090 MHz.

The two sources of data during the test flights were the Nike tracking data tape and the sensor's data collection tape. The tracker tape contained the range, azimuth (referenced to true north), and elevation angle of the target updated every 0.1 second. The sensor's data collection tape contained the time-tagged (time of day) ATCRBS and Mode S target reports of the test aircraft. The target reports were composed of the aircraft's ATCRBS or Mode S code (depending on the target report type), the aircraft's range from the sensor, altitude, the monopulse value of the reply, and the target bearing in AU's. To facilitate filtering of the ATCRBS target reports a unique code was assigned to the test aircraft.

Throughout the test flights the times of day recorded on the Nike tracker tape and the sensor's data collection tape were synchronized with the WWVB transmissions of the NBS facility at Boulder, Colorado.

INTERFERENCE TESTS. The basic procedure followed in the interference tests was to inject simulated fruit at the RF level into the front-end of the sensor and to collect data using the RAA diagnostic. The fruit for performing these tests was generated by two pieces of specialized test equipment previously used at the Technical Center for similar interference work. The first was an ATCRBS fruit generator that can provide up to 40K ATCRBS ATCRBS fruit/sec. The second fruit generator was designed at the Technical Center for producing Mode S fruit.

The basic test setup for performing the interference tests is shown in figure 9. For each type of fruit the ouput of the particular fruit generator was used to modulate a 1090 MHz source. The resulting signal was then fed into an RF network that provided the appropriate sum and difference signals for a given off-boresight angle.

TABLE 2

FLIGHT PLAN FOR PHASE AND AMPLITUDE MONOPULSE COMPARISON

Flight Type* (Radial/Orbit)	Altitude (feet)	Range (nmi)
Radial	20,000	5-40
Radial	15,000	5-40
Radial	11,000	5-40

*All radials were along a 151 degree true north radial centered on the Mode S sensor.

INTERFERENCE TEST SETUP

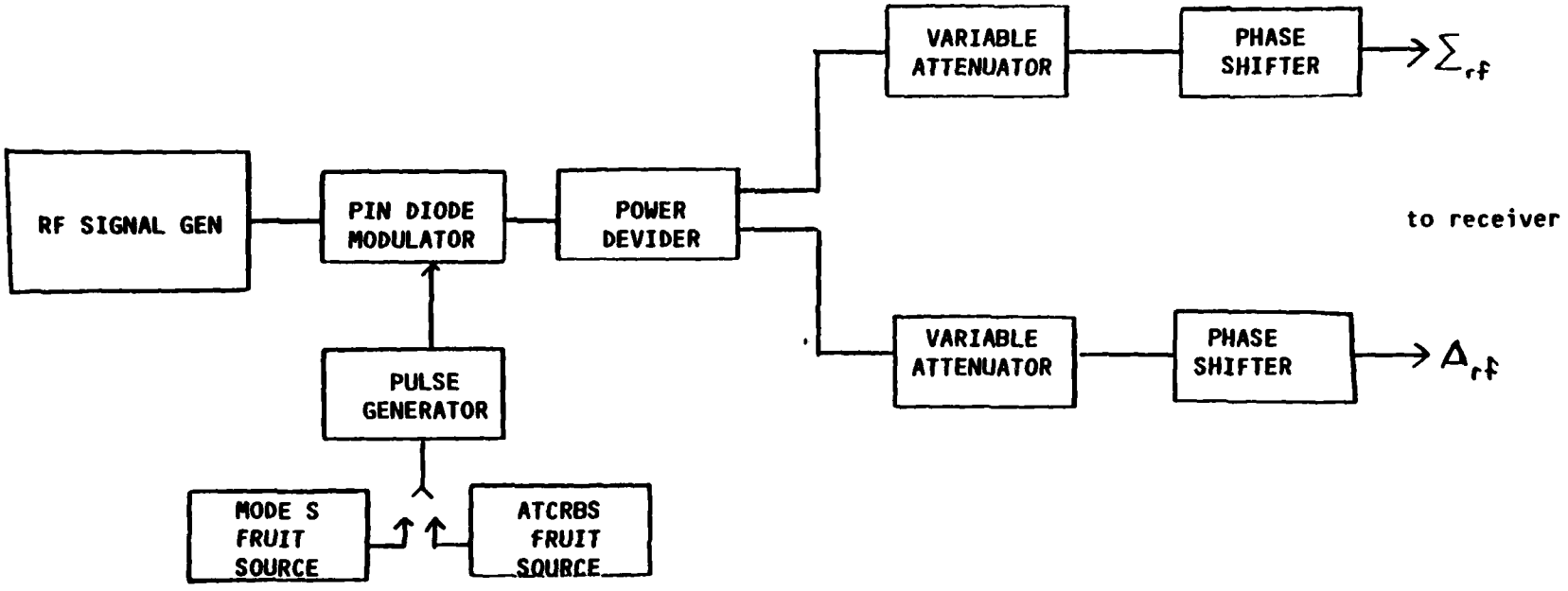

FIGURE 9

The characteristics of the fruit were held constant for the period of time that it took for the RAA to collect 64 complete scans of data on the CPME. Due to the definition of the SIR used for these tests, a given SIR value resulted in differing amplitudes for the fruit. A correction table was generated based on the antenna plots for the 5-foot open array to permit inputting the correct interference amplitude for different {D}/{S} ratios. These corrections are shown in table 3.

Preliminary data was taken to ascertain the effects of fruit at differing signal-to-noise ratios (SNR). For a SNR of 40 dB, at SIR's of +20 and +10 dB the fruit rate was 200 Mode S per second. At a SIR of 0 dB the rates were 50, 100, and 200 Mode S fruit per second. Since the effects of fruit under these conditions were negligible, a SNR of 25 dB, the lowest possible at which the sensor could be calibrated, was used in the rest of the tests.

At an SNR of 25 dB the fruit rates were 1.6K, 5K and 16K for ATCRBS and 100/sec for Mode S. At each of these rates data were collected using SIR's of -10, 0, and +10 dB at each of the points in the beam: the +6 dB point, crossover, and boresight. Also, for 16k ATCRBS, a worst case test was made using an SIR of -20 dB.

TABLE 3

D/S AND SIR CONVERSION TABLE

Angle(D/S)	SIR db			
	-10	0	+10	+20
-30 dB	+10	0	-10	-20
0 dB	+7	-3	-13	-23
+6 dB	+2	-8	-18	-28

dB down from boresight for interference

DATA REDUCTION

The data analysis for the various phases of this test program are presented below. The flight check data were collected and reduced using software programs developed previously during the Mode S T&E program and processed on the Technical Center's Honeywell 66/60 general purpose computer.

The ground accuracy and interference test data were collected using the Mode S system RAA program, and reduced on a PDP 11/45 computer using software also developed under the Mode S T&E program at the Technical Center.

Data from the static tests were processed using a Tektronix 4054 desktop computer with software developed under this effort.

STATIC TESTS. The results of these tests are a series of plots relating each of the measured log {S}, log {D}, and {D}/{S} outputs to the input signal strength, relative signal strength {D}/{S}, and reply frequency.

GROUND ACCURACY TESTS. These tests, as noted earlier, were subdivided into accuracy tests, off-frequency tests, and low power tests. The analysis planned for each was essentially the same and utilized existing reduction software. The primary analysis was for the purposes of establishing azimuth accuracy of both receivers and determining azimuth error as a function of reply frequency and received power. The specific measures that resulted were the mean error and the deviation of the equivalent monopulse angle in AU's. These were plotted as a function of actual bearing of the CPME and encompassed angles exceeding the {S} and {D} crossover points. For these tests the RAA program was used to collect the data, while a separate data reduction program generated the plots.

Off frequency and low power error plots were generated in the same manner as the plots for the 1090 MHz ground accuracy tests.

FLIGHT TESTS. The data collected during these tests were processed to derive the residual differences in the angular determination by the Mode S sensor and that of the Technical Center's Nike tracking facility. The data tapes from the tracker and the sensor were merged and the relevant accuracy plots generated using the reduction program developed during the initial "Mode S Accuracy Tests" (reference 3). The results of this processing were a set of histograms for azimuth residuals along with the resulting mean and standard deviation for Mode S and ATCRBS replies when operating with the unmodified and modified receivers.

INTERFERENCE TESTS. The interference data was reduced using the same DR& A software utilized for the Ground Accuracy tests, giving the mean error and standard deviaiton of the fruit affected replies. The average number of replies per beam (two scans) for each SIR was tabulated using the printouts from the RAA data collection Program, RAATPD (reference 9).

RESULTS AND ANALYSIS

STATIC TESTS

RECEIVER RESPONSE. The receiver response characterisics are presented in Figures 10 to 12. The first figure is a result of the data collected using the pulsed RF test setup and shows the amplitude response of the log amplifiers in the amplitude receiver, i.e., the slopes of the two curves are approximately 55 mV/dB. As would be expected some ripple is detectable in the individual curves, with the most notable areas occuring at less than -65 dBm. Some compression can also be noted between -20 and -30 dBm. In order to demonstrate the ripple that exists between the two outputs, the outputs of the two amplifiers nave been subtracted from each other in figure 10B. The ripple present present is approximately equal to 150 mV.

Figure 11 plots the delta/sum outputs of both receivers as a function of input power at the different {D}/{S} input ratios. These plots were generated using the data from the basic CW tests. From the plots it is apparent that the variations for the amplitude receiver far exceed those of the phase receiver. Based on the approximate slope of the response of the log amplifiers (55 mV/dB), overall variations in excess of 1 dB are readily detectable (the voltage increments in the plots are 59 mV/dB each). The sharp variations that occur at -25 to -30 dBm are with {D}/{S} ratios of from -15 to +6 dB and are due primarily to the compression of the log amplifiers.

The fact that the phase receiver is not dependent upon the characteristics of the log amplifiers is exemplified by the relative insensitivity of the delta/sum ratios with variations in received power. The results for the phase receiver also indicate that sufficient signal remains present at the input to the phase detectors to provide a well behaved delta/sum ratio. This is due to the limiting amplifiers that precede the phase detectors in the half-angle processor.

The characteristics of the actual monopulse video, MRMVD, for both receivers are shown in figure 12. The curves were derived from pulsed input signals with a {D}/{S} ratio of 0 dB. Again, ripple is noticeable for the amplitude receiver over the power range tested. Since the A/D converter digitizes into 256 discrete levels over an input range of approximately 0 to -2.55 volts, a 10 mV variation in the MRMVD will result in a variation of one monopulse unit.

BANDWIDTH. The results of the bandwidth measurements are presented in Figures 13 to 14. The overall results of the CW tests are presented in Figure 13 which shows the output of the {D}/{S} channel for both receivers over the power range of -25 to -80 dBm at a {D}/{S} input ratio of 0 dB. The variation of the delta/sum output with frequency and power are more noticeable in the amplitude receiver than in the phase receiver. The ripple in the output for the amplitude receiver arises due to frequency response, while the up and down movement of the amplitude curves are attributable to the variation in power. It was determined from figure 13 that the ripple with frequency averaged approximately 25 to 50 mV. A slight slope for the phase receiver can be detected with increasing frequency in figure 13.

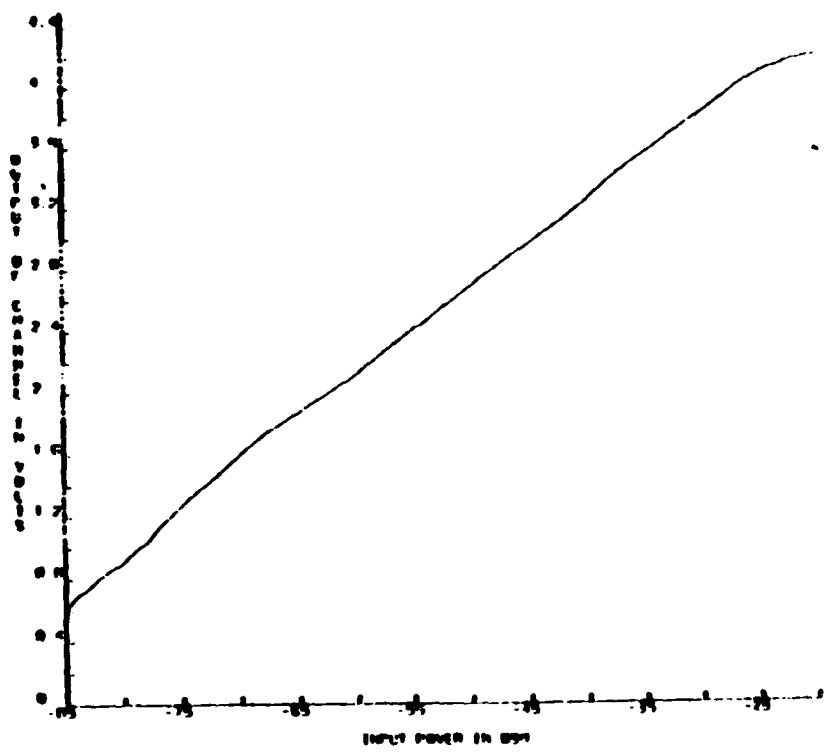

FIGURE 1. DELTA LOG AMPLIFIER OUTPUT (1/25/82)

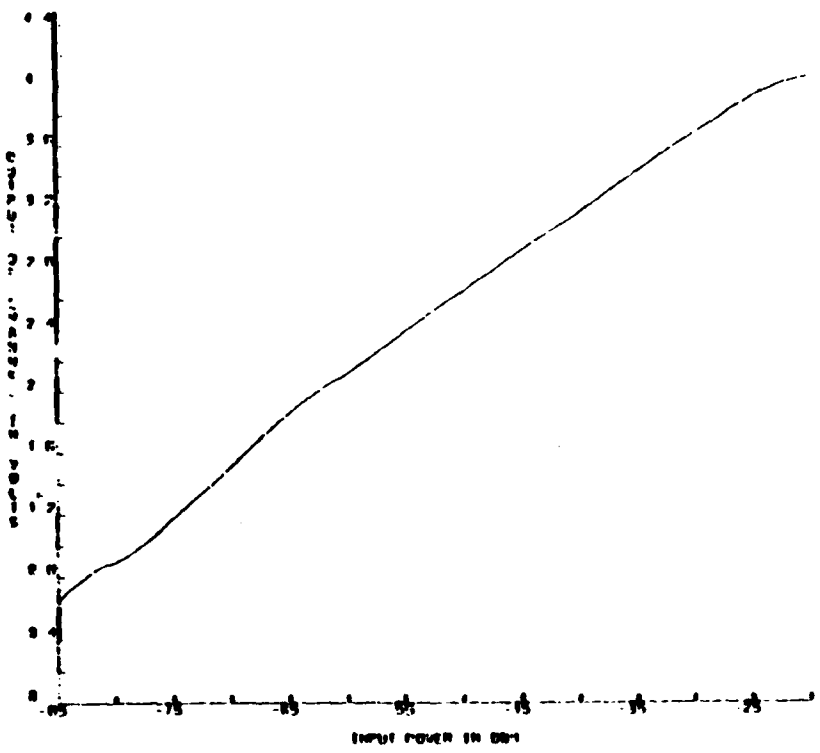

FIGURE 2. SUM LOG AMPLIFIER OUTPUT (1/26/82)

FIGURE 10A. RECEIVER RESPONSE

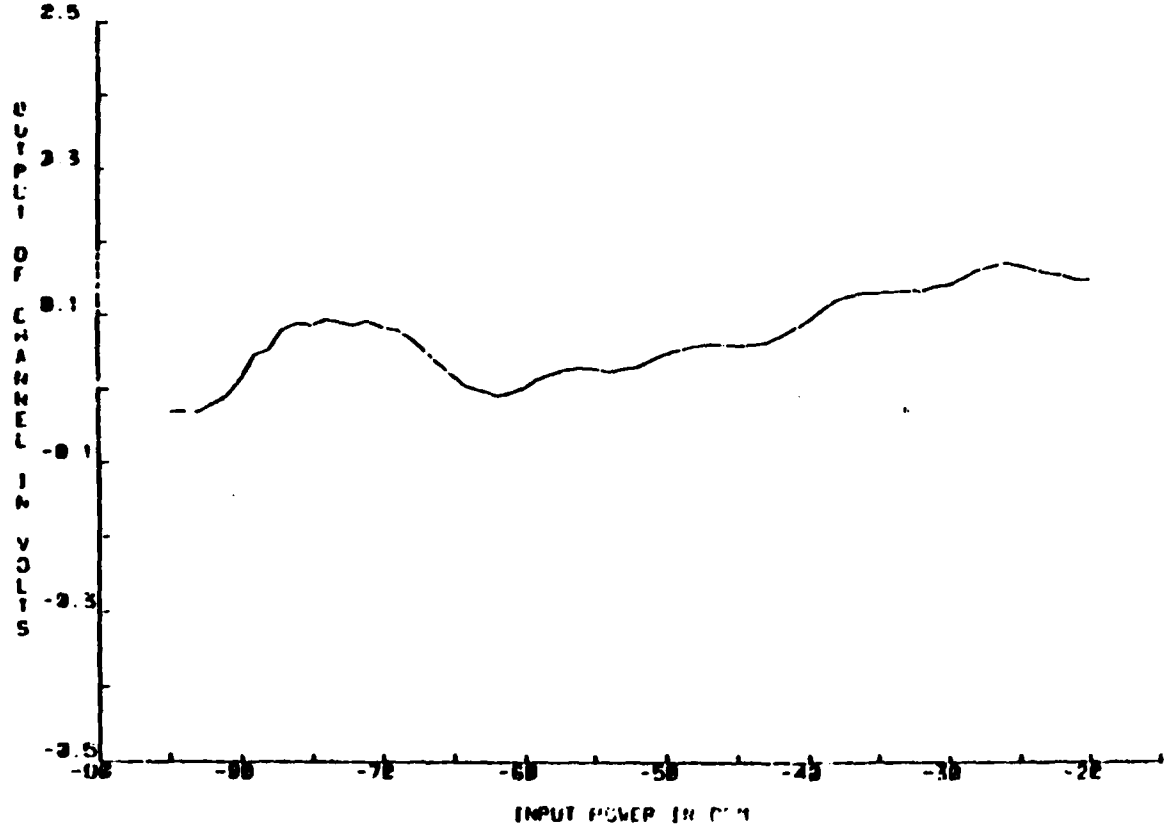

FIGURE 10B LOG(DELTA)-LOG(SUM) OUTPUT

CH Y CH M

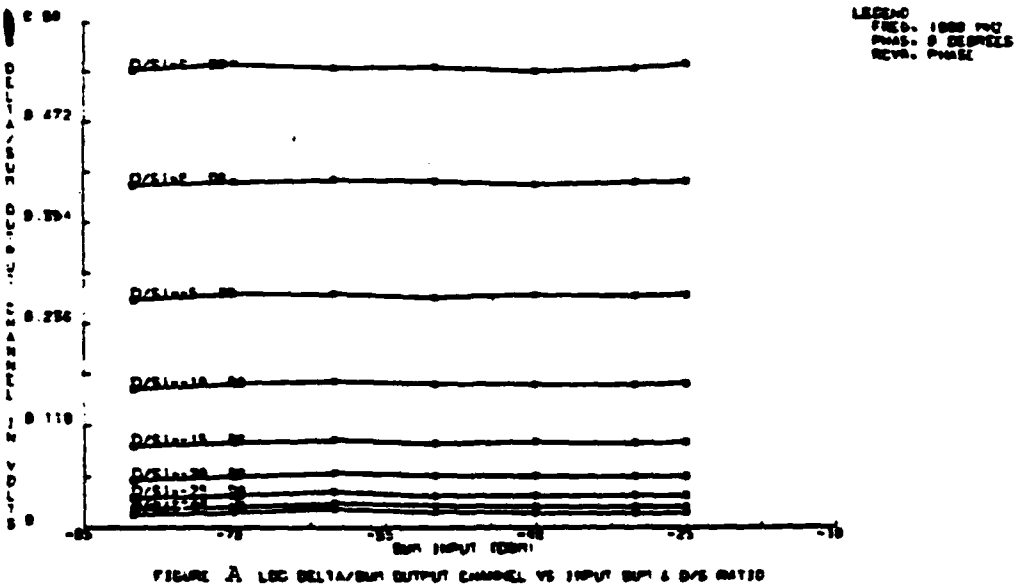

FIGURE A LEC DELTA/SUM OUTPUT CHANNEL VS INPUT SNR & D/S RATIO

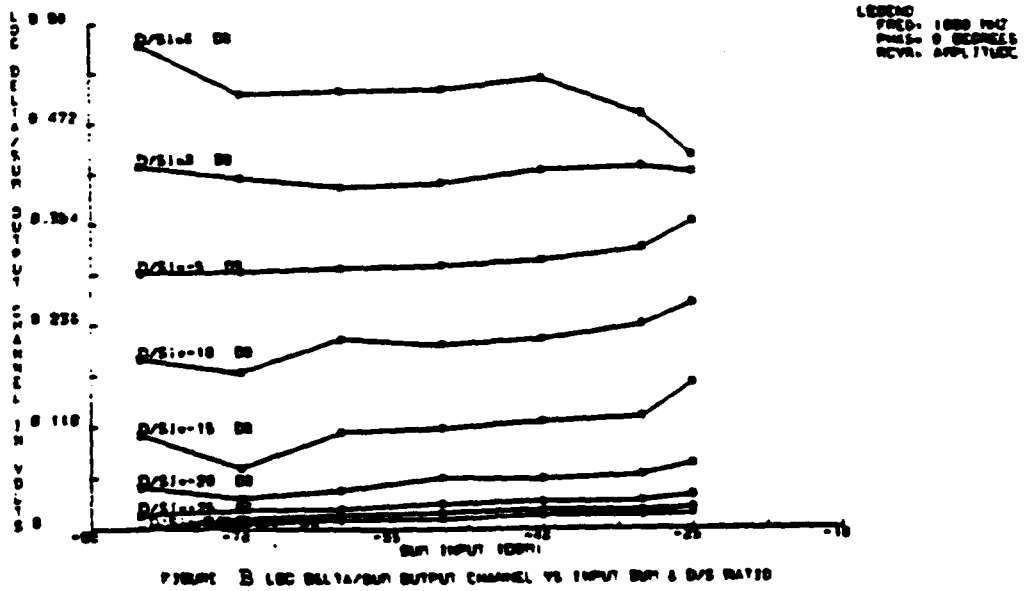

FIGURE B LEC DELTA/SUM OUTPUT CHANNEL VS INPUT SNR & D/S RATIO

FIGURE 11. RECEIVER RESPONSE

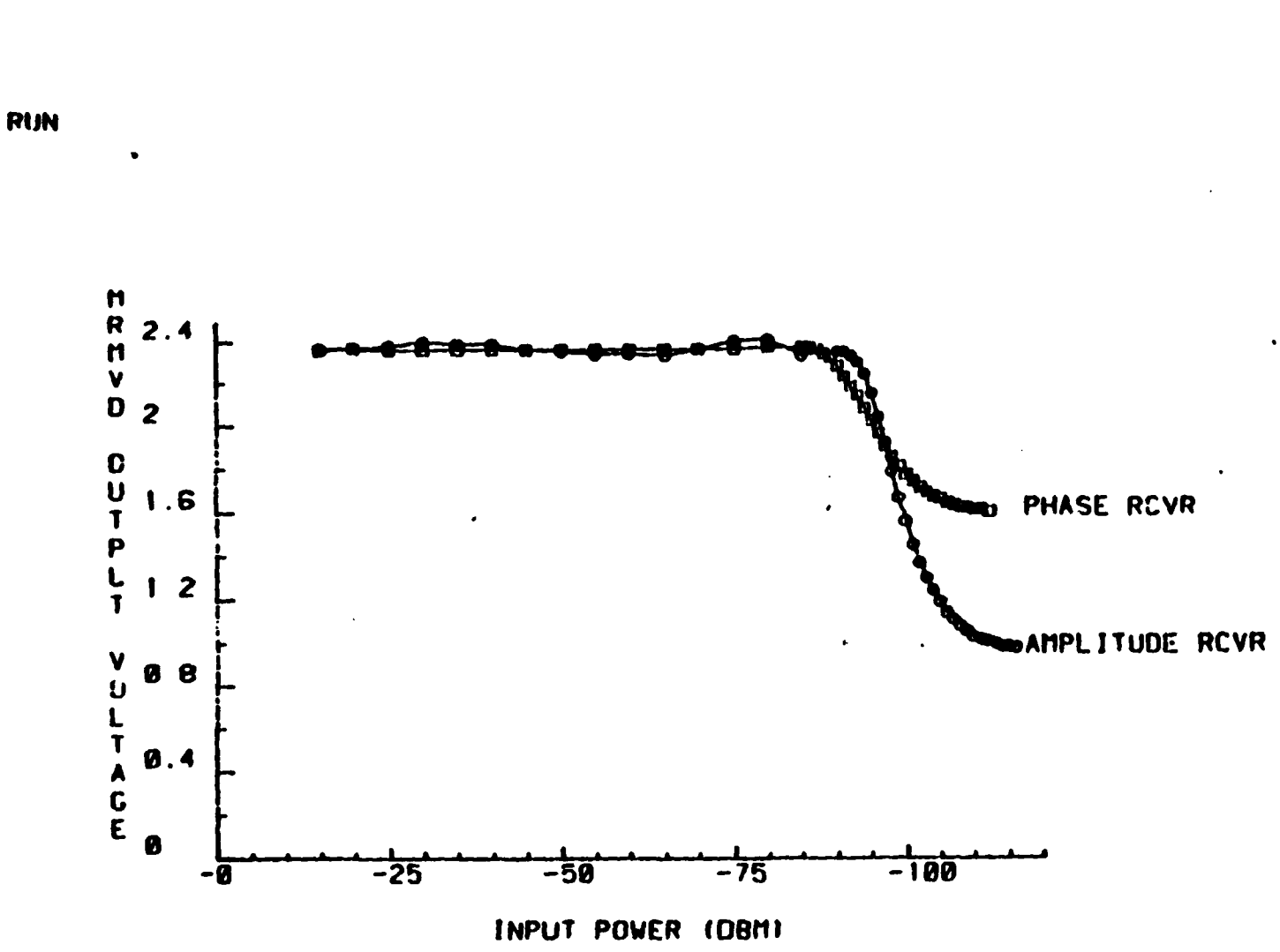

FIGURE 12. PHASE AND AMPLITUDE MONOPULSE VIDEO VS INPUT POWER

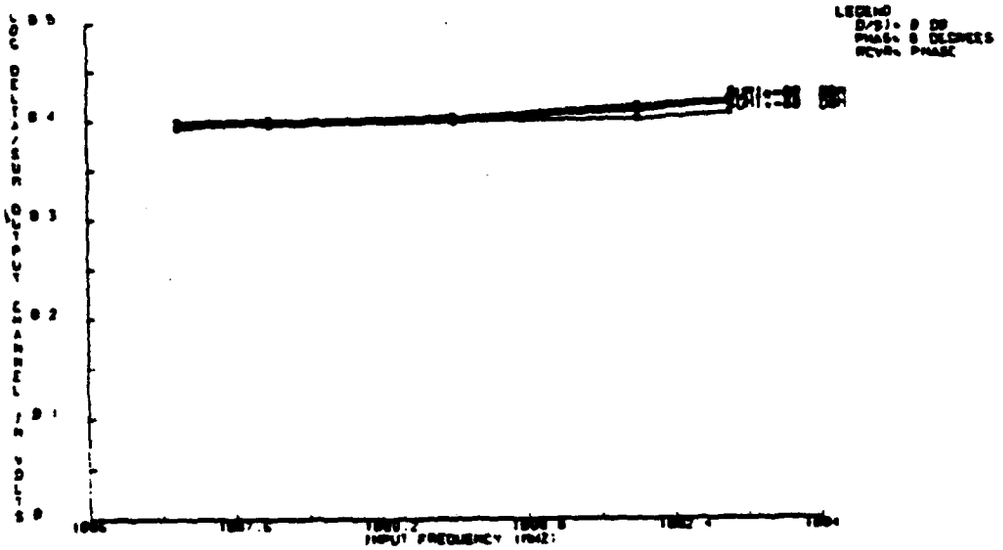

FIGURE 1 LOC DELTA/SUM OUTPUT CHANNEL VS INPUT FREQUENCY & SUM

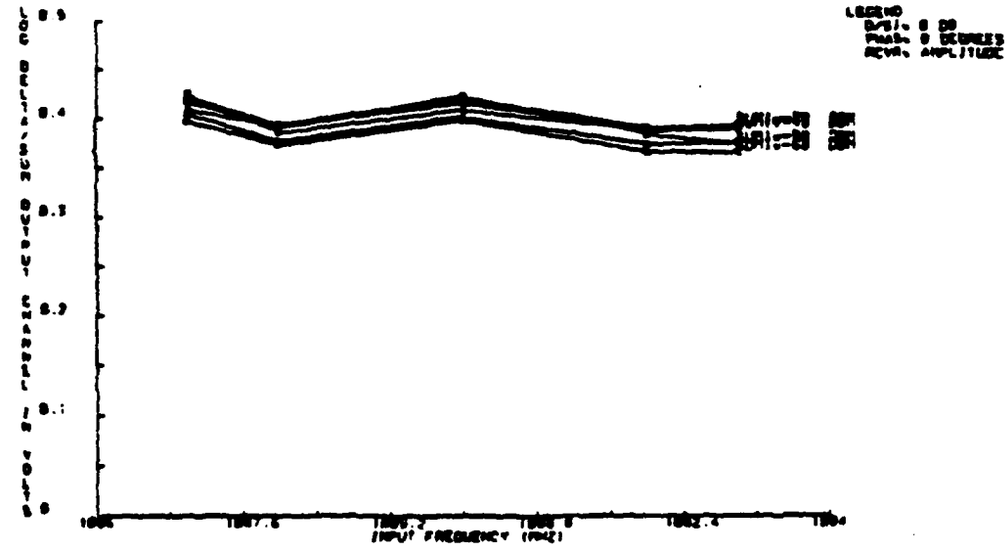

FIGURE 2 LOC DELTA/SUM OUTPUT CHANNEL VS INPUT FREQUENCY & SUM

FIGURE 13. RECEIVER BANDWIDTH

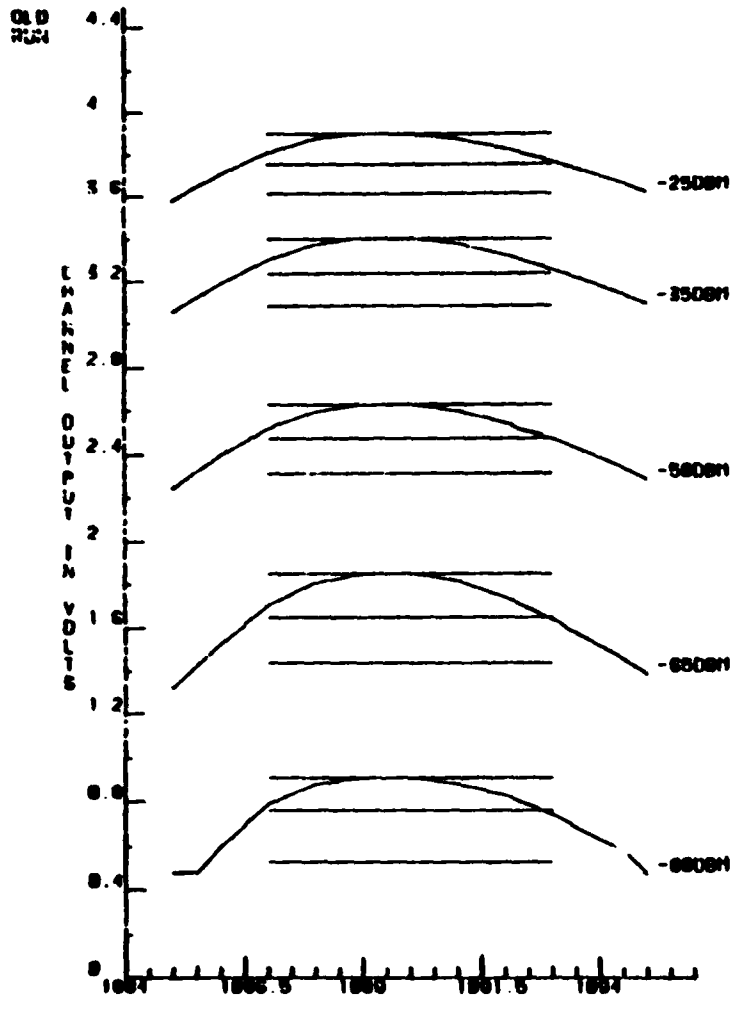

FIGURE .1 SUM LOG AMPLIFIER BANDPASS AT DIFFERENT INPUT RF LEVELS

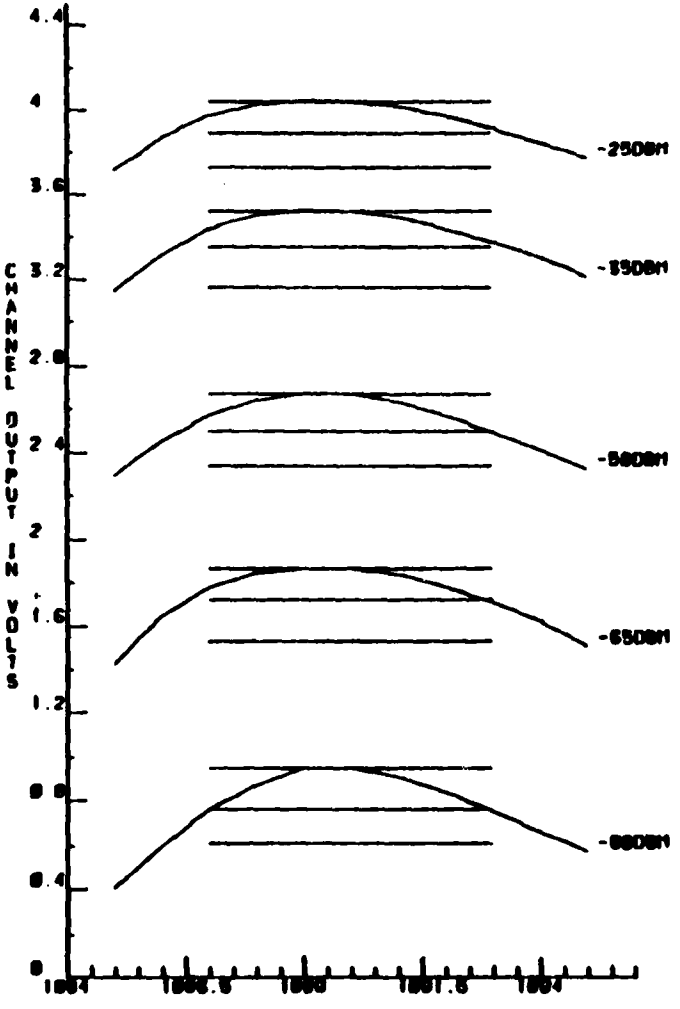

FIGURE .2 DELTA LOG AMPLIFIER BANDPASS AT DIFFERENT INPUT RF LEVELS

FIGURE 14A. RECEIVER BANDPASS

The results in figure 14 were obtained using a pulsed RF input and a (D)/(S) ratio of 0 dB. The point of measurement (log amp outputs) makes the plots independent of receiver type. Horizontal lines have been drawn to mark the 0, 3, and 6 dB points at 1090 mHz and for each power level. The overall frequency response of both channels (3 dB points) were for the sum channel 1087 to 1093 MHz, and from 1087 to 1092.8 MHz for the delta channel. The differnces, i.e., log(D)-log(S), at each power level as a function of frequency is shown in figure 14B. The overall variation is approximately 200 mV.

RECEIVER TRACKING. The ability of the sum and delta channels to track each other over a wide power range is of critical importance in generating a consistent monopulse value. Figure 15 shows the results of the tracking tests performed on both receivers. Generated using data collected during the basic CW testing, the figure plots (D)/(S) outputs for each receiver at each input power level and for in phase and out of phase conditions, i.e., right and left of boresight. The results for the phase receiver demonstrate the tight tracking needed over -20 to -80 dBm input power to provide a reliable off boresight estimate. The results for the amplitude receiver reveal relativily wide variations based on input power levels. This is particularly true in the mid range of delta/sum ratios, i.e., areas between boresight and the crossover point. The variations narrow at the crossover point and then begin to diverge beyond that point. This variation wa attributed to two factors. The first was the ripple in the log amplifiers due to the limited number of stages, seven, and the alignment procedure used to setup the log amplifiers. In order to minimize the ripple in the two log amplifiers a CW signal was injected via a Voltage Controlled Attenuator (VCA), figure 6. With equal power into each channel of the amplitude receiver the input power to each channel was varied from -20 to -90 dBm. The resulting curves, shown in figure 16 were monitored on an oscilliscope and the log amplifiers adjusted to provide an overall variation of +/-1 dB ripple. After minimizing the ripple, the input power to the delta channel was varied over +6 to -35 dB, with respect to the sum channel. The output curves were then monitored to assure that the +/- 1 dB was maintained. Since the adjustment of the amplifiers was performed using an input RF signal rather than at IF, it did not exclude possible variations in component characteristics prior to the log amplifiers. The precise cause of the reduced variations that occur at the crossover have yet to be identified. It should be noted, however, that the overall variation of the delta/sum ratio in figure 15 is 120 mV, i.e., +/- 1 dB. As a point of refernce the output of the sum log amplifier has also been included in figure 16.

RECEIVER DETECTION. ATCRBS bracket detection for the two receivers was performed using simulated ATCRBS inputs at 1090 MHz. The results of those measurements are shown in figure 17. The 90 percent detection point for the amplitude receiver was -82 dBm, while the sensitivity for the phase receiver was -78 dBm.

GROUND ACCURACY TESTS

The ground accuracy data are presented as a series of azimuth error plots. The plots show both the mean azimuth error, shown as dashed lines, and the +/- 1 sigma standard deviation, shown as solid lines. The error is in azimuth units (0.022 deg/AU) and is plotted versus position in the beam, which is also in AU's (128 AU's being equivalent to boresight). Each plotted point is comprised of from 20 to 40 samples.

PLOT OK Y OR N

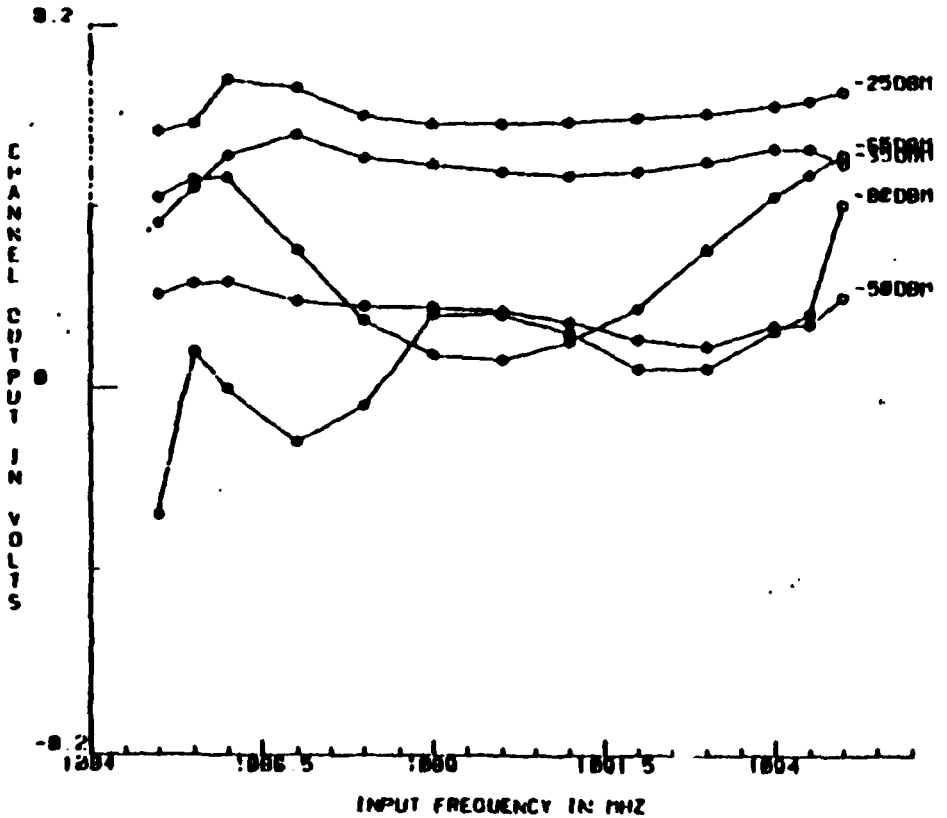

FIGURE 14B DELTA-SUM LOG AMPLIFIER BANDPASS AT DIFFERENT INPUT RF LEVELS

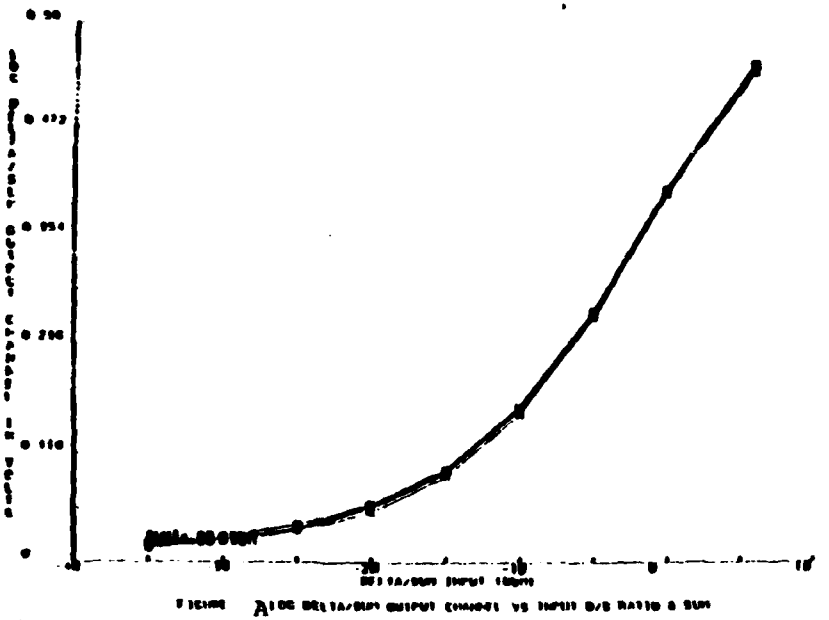

A

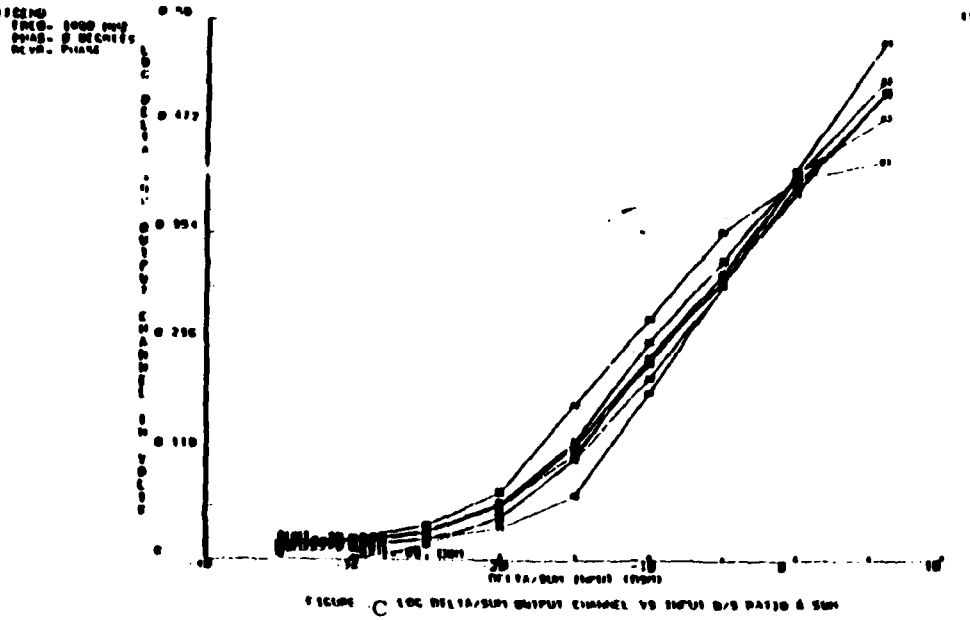

C

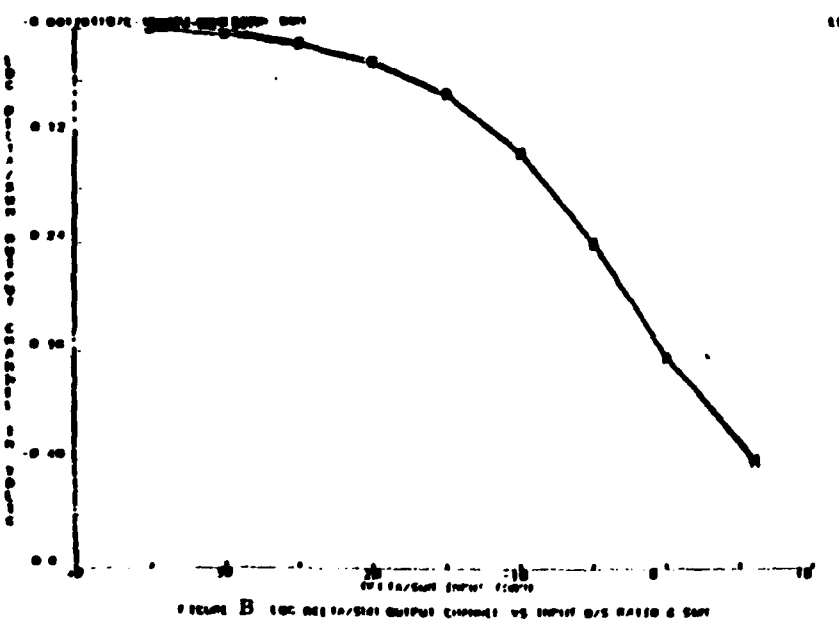

B

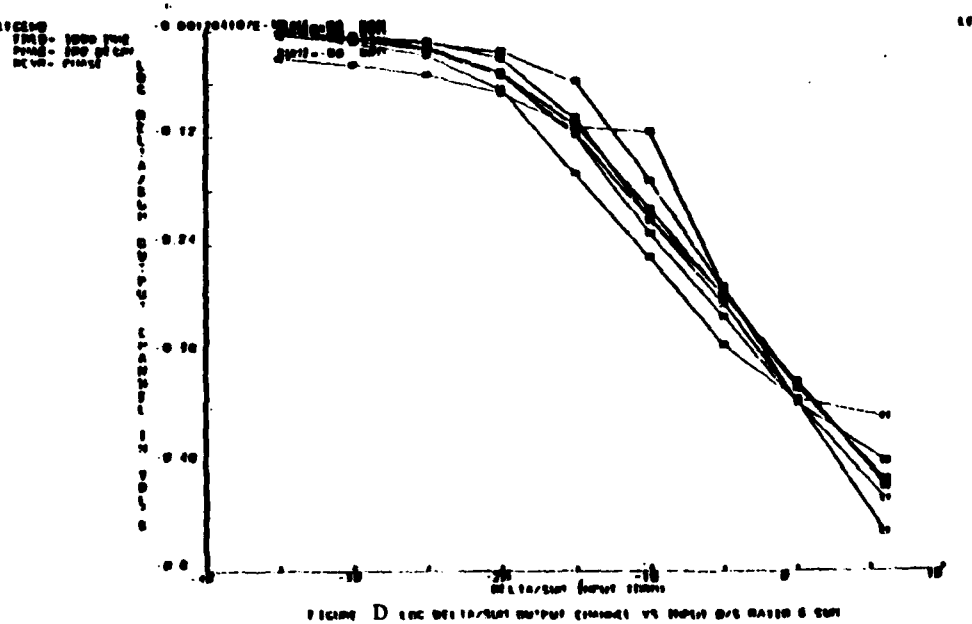

D

FIGURE 15. RECEIVER TRACKING

LOG AMPLIFIER TRACKING PHOTOGRAPHS

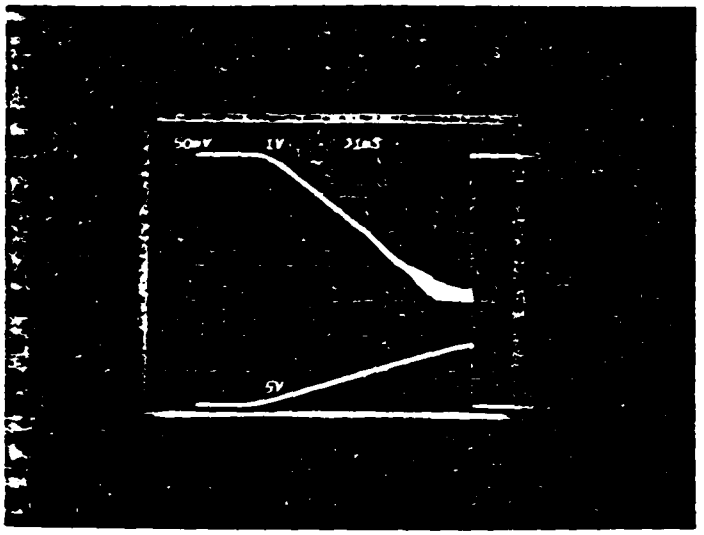

PHOTO #1
TOP TRACE: LOG SUM VIDEO OUTPUT

BOTTOM TRACE: CONTROL VOLTAGE INPUT TO V.C.A.

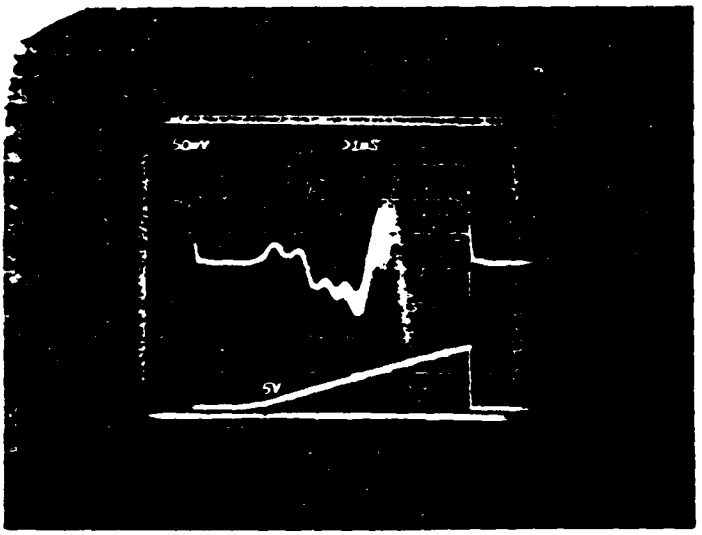

PHOTO #2
TOP TRACE: LOG DELTA - LOG SUM USING TEKTRONIX DIFF AMP
RF INPUT=-20 TO -90 DBM
BOTTOM TRACE: CONTROL VOLTAGE INPUT TO V.C.A

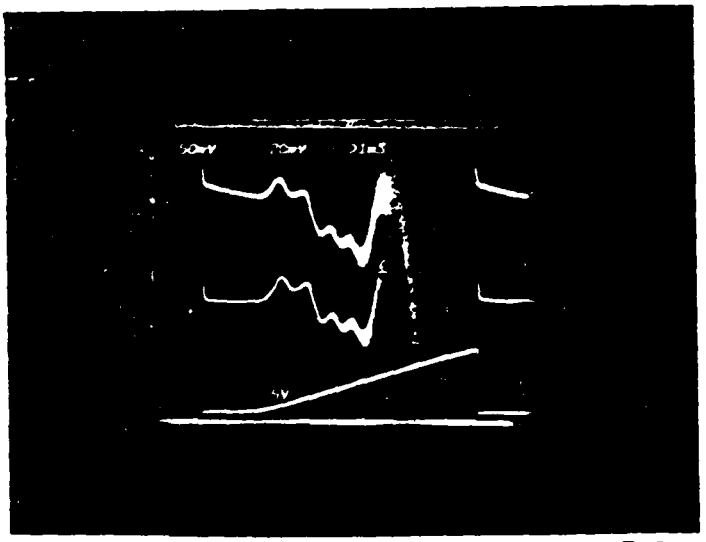

PHOTO #3
TOP TRACE. DELTA/SUM OUTPUT OF AMPLITUDE RECEIVER
MIDDLE TRACE: LOG DELTA - LOG SUM USING TEKTRONIX DIFF AMP
BOTTOM TRACE: CONTROL VOLTAGE INPUT TO V.C.A.

FIGURE 16

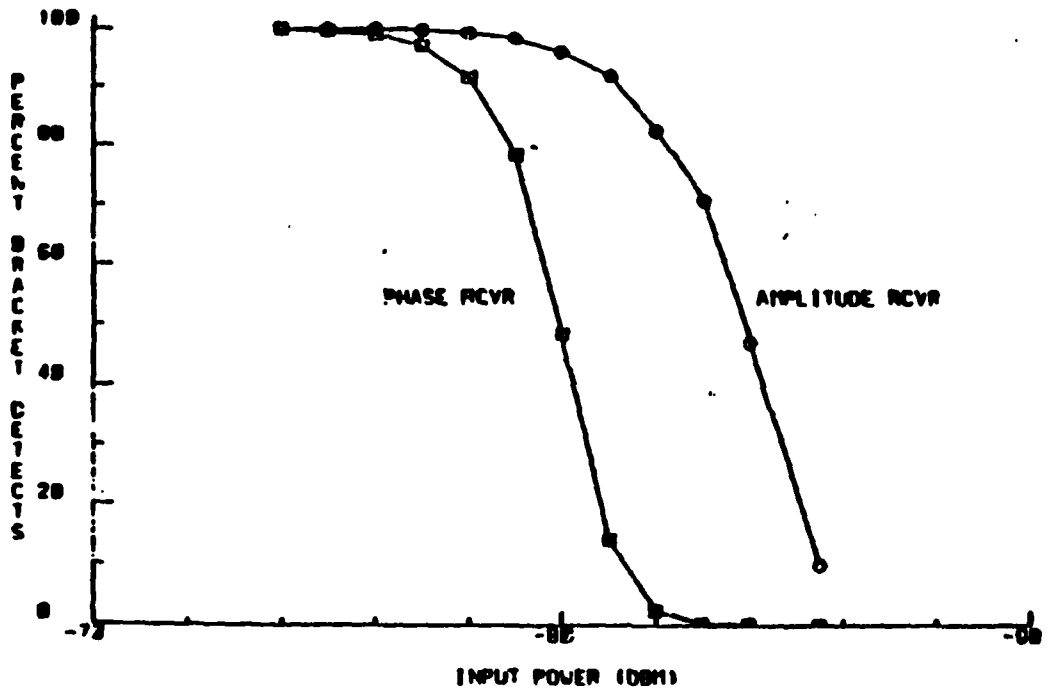

FIGURE 17 PHASE AND AMPLITUDE MONOPULSE BRACKET DETECTIONS

AZIMUTH ACCURACY. The data collected on the azimuth accuracies of the phase and amplitude receivers are shown in figure 18. The data were collected over as wide a beamwidth as possible. This was accomplished by lowering the thresholds which limit the delta to sum ratio (Td) and the omni to sum ratio (To). The result was a 4.75 degree beamwidth in the phase receiver and a 4.8 degree beamwidth in the amplitude. The tests were performed using a received signal strength of -54 dBm and 1090 MHz.

The azimuth error of both receivers was less than 1 AU over most of the beam and no greater than 2 AU's at any point in the beam. The standard deviation of both receivers was generally less than 2 AU's with only occasional spikes of appoximately 4 AU's.

OFF FREQUENCY. The off frequency azimuth error data for both receiver types is presented in figures 19A and 19B. The mean data for each frequency has been consolidated into one plot for comparison purposes. The standard deviation curves for each receiver-frequency combination is not shown in these plots. However, the standard deviation for both receivers at all frequencies was consistently less than two AU's.

The effective received power used during the testing with the phase receiver was restricted to -59 dBm at 1090 MHz. This limitation was dictated by the maximum power available with the RF signal generator used to replace the CPME's RF source. During the tests with the amplitude receiver the effective power for each frequency was seperately established at approximately -63 dBm. This approach was taken to try and minimize the errors that arise due to power variations (discussed in the Power Variations section of this report). The specific power level was established by the maximum power available from the signal generator at which all the frequencies under investigation would result in the same effective power at the sensor.

Results for the phase receiver show a variation of mean error of +/- 4 AU's in the range of 1088 to 1093 MHz. The mean error tends to increase rapidly, particularly at the beam edges for 1087, 1086, and 1094 MHz. The errors in these cases equal or exceed 8 AU's. An approximate 1 AU offset is present at boresight for the higher frequencies, i.e., 1092 to 1094 MHz. Results of the tests are generally consistent with the results of prior off-frequency tests performed on the Mode S sensor (reference 5).

The amplitude receiver had a maximum mean error over 1094 to 1086 MHz of +/-4 MHz. The plots of the mean errors show a generally linear characterstic that consistently has a zero mean error at boresight and increases with off-boresight angle for several of the frequencies. This phenomena is a result of frequency dependent gain imbalances in the <S> and <D> channels. This dependence does not, however, bear a one to one relationship with frequency, i.e., higher frequencies do not cause consistently higher or lower errors.

LOW POWER. The low power data (figures 20 and 21) show the effects that low level replies have on azimuth accuracy. The CPME transmit signal was lowered to provide an effective received power at the sensor of -70 dBm at which point the amplitude receiver was calibrated, i.e., the level at which the monopulse curve was established. This was done in order to minimize the impact of the ripple that was known to exist in the tracking between the two amplifiers. It should be noted in reviewing the plots that the calibration for the phase receiver was performed at -54 dBm. Once calibrated the tests were performed at -70, -76, -78, and -79 dBm receive signal level.

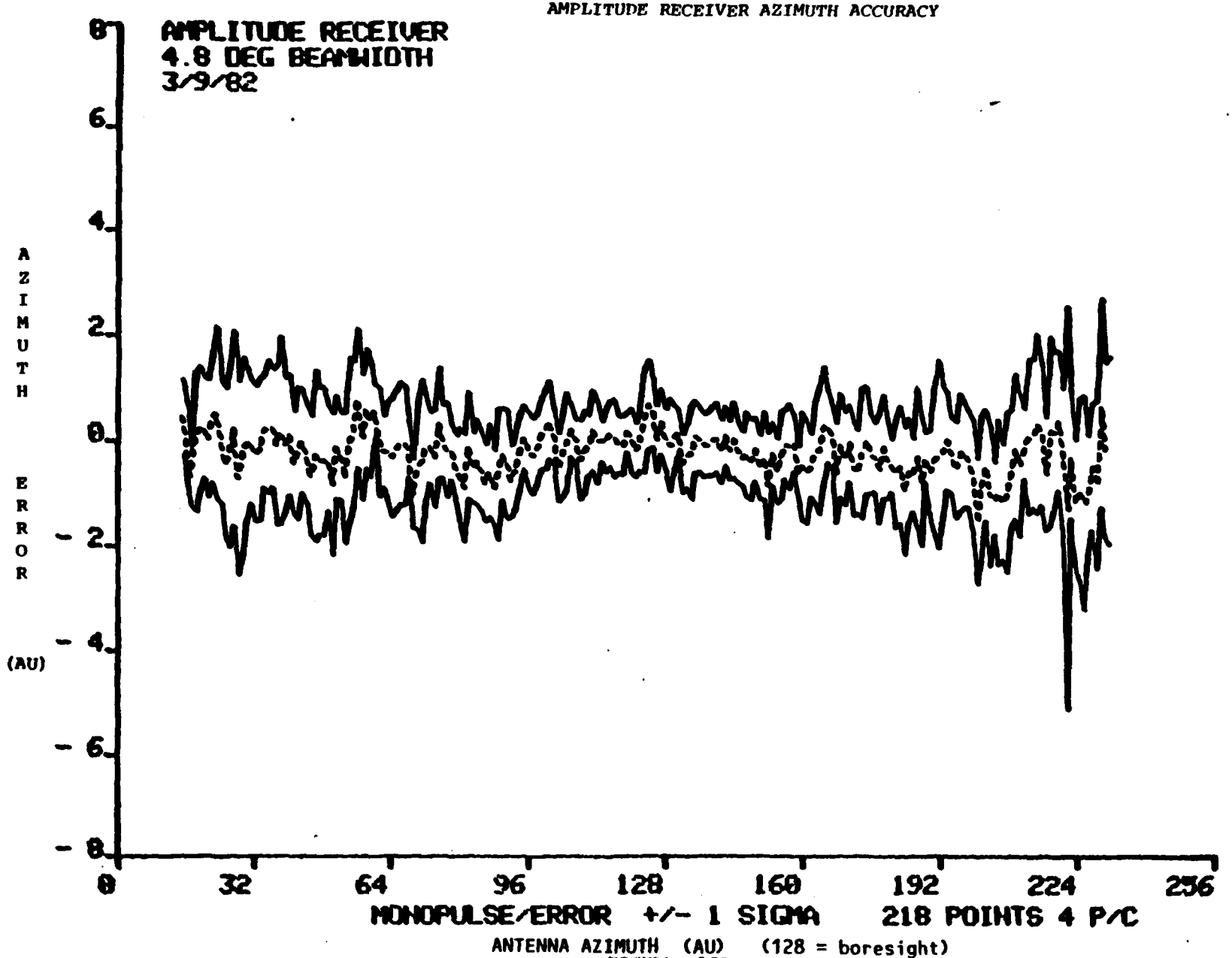
AMPLITUDE RECEIVER
4.8 DEG BEAMWIDTH
3/9/82
AZIMUTH ERROR (AU)
8
6
4
2
0
- 2
- 4
- 6
- 8
0
32
64
96
128
160
192
224
256
MONOPULSE/ERROR +/- 1 SIGMA 218 POINTS 4 P/C
ANTENNA AZIMUTH (AU) (128 = boresight)

FIGURE 18A

AMPLITUDE RECEIVER MONOPULSE CURVE

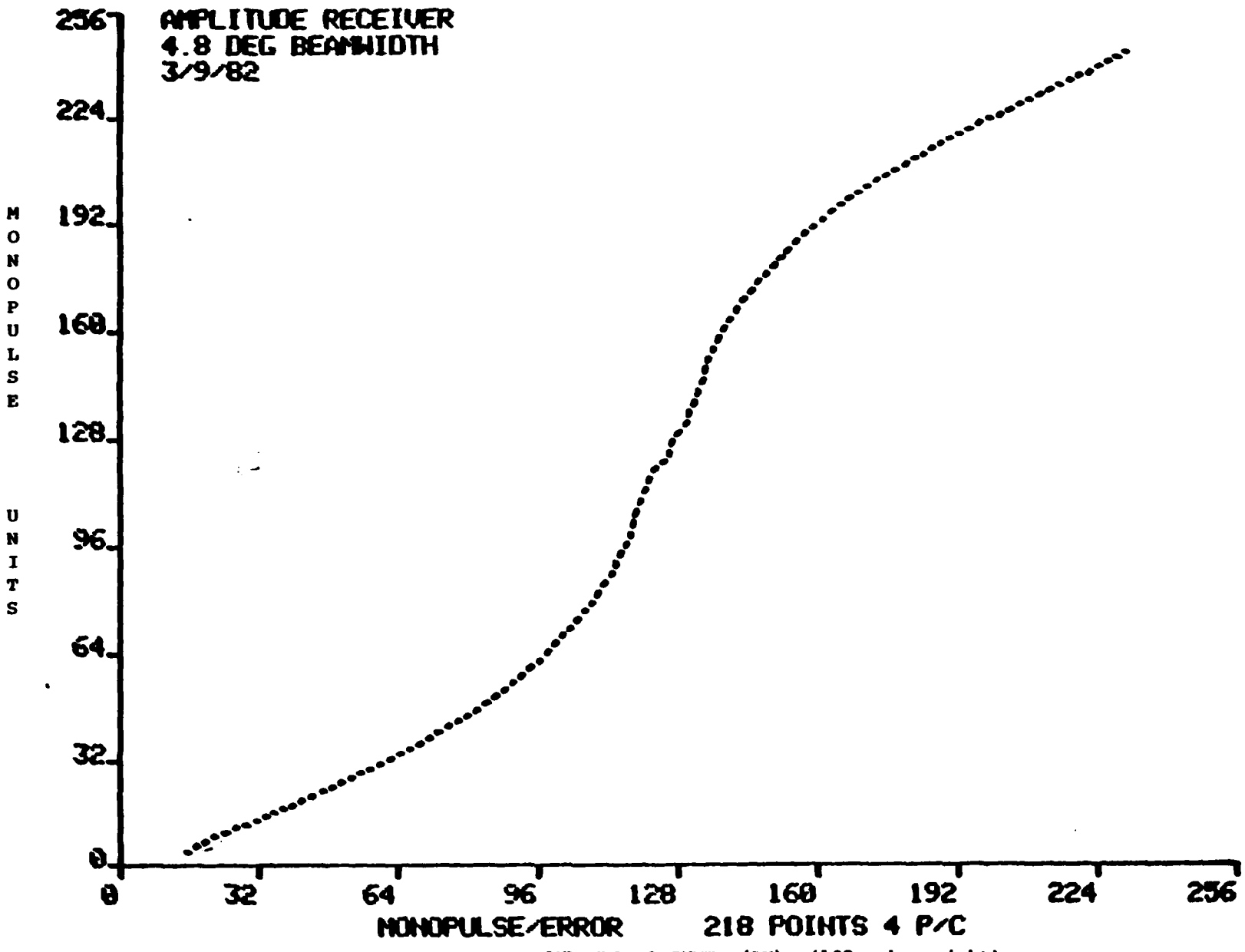

ANTENNA AZIMUTH (AU) (128 = boresight)

FIGURE 18b

PHASE RECEIVER AZIMUTH ACCURACY

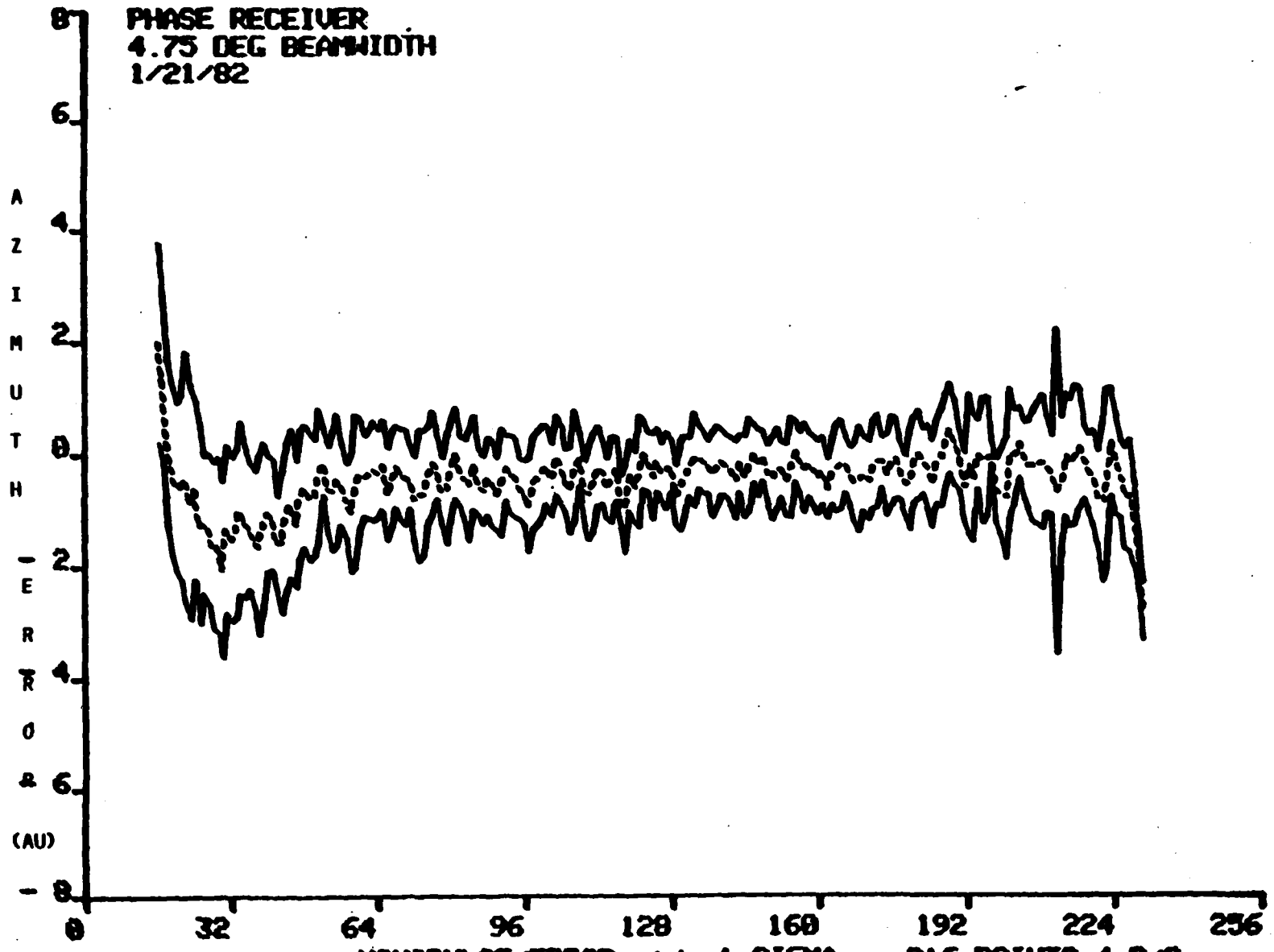

FIGURE 18c

PHASE RECEIVER MONOPULSE CURVE

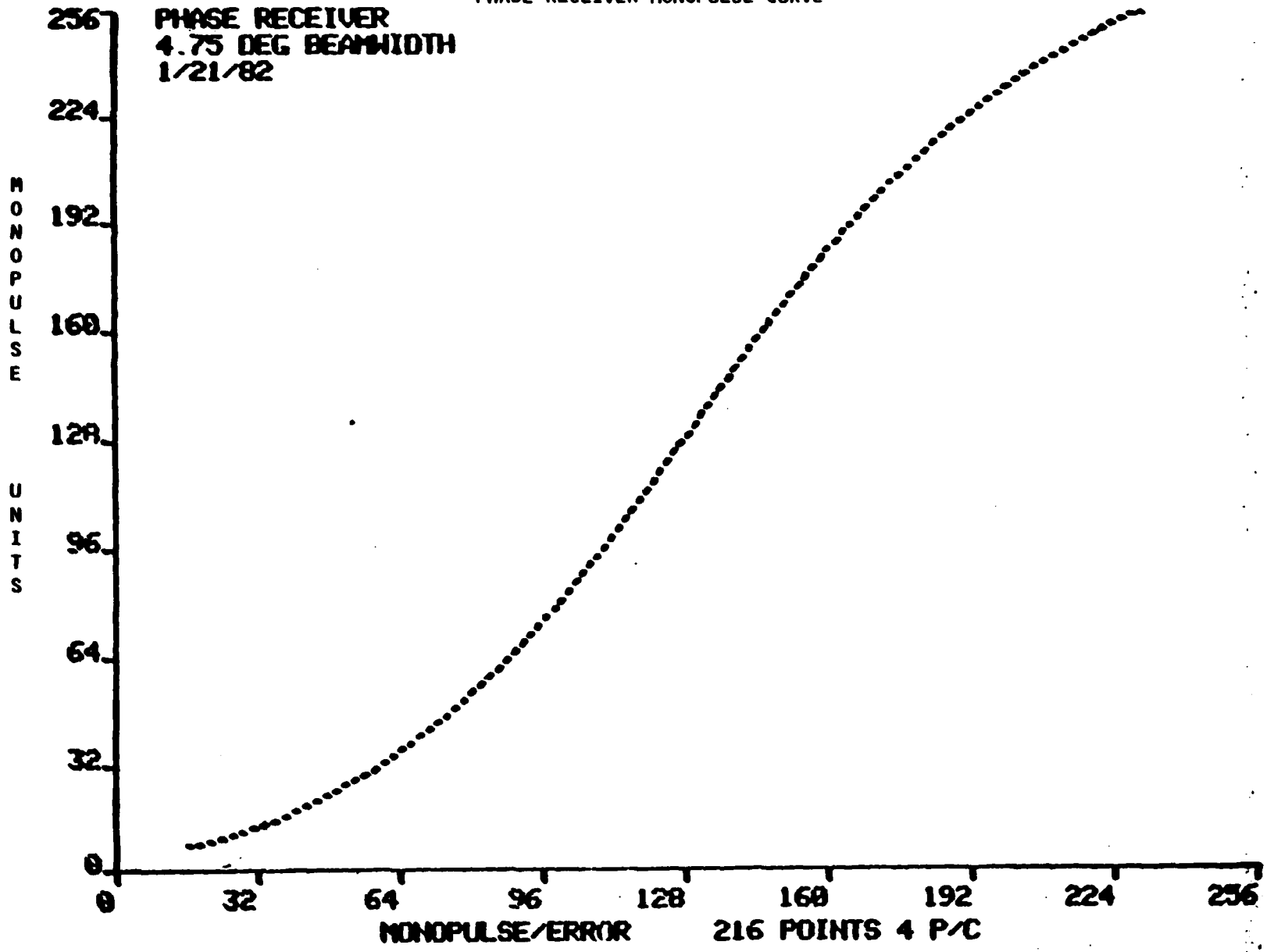

FIGURE 18d

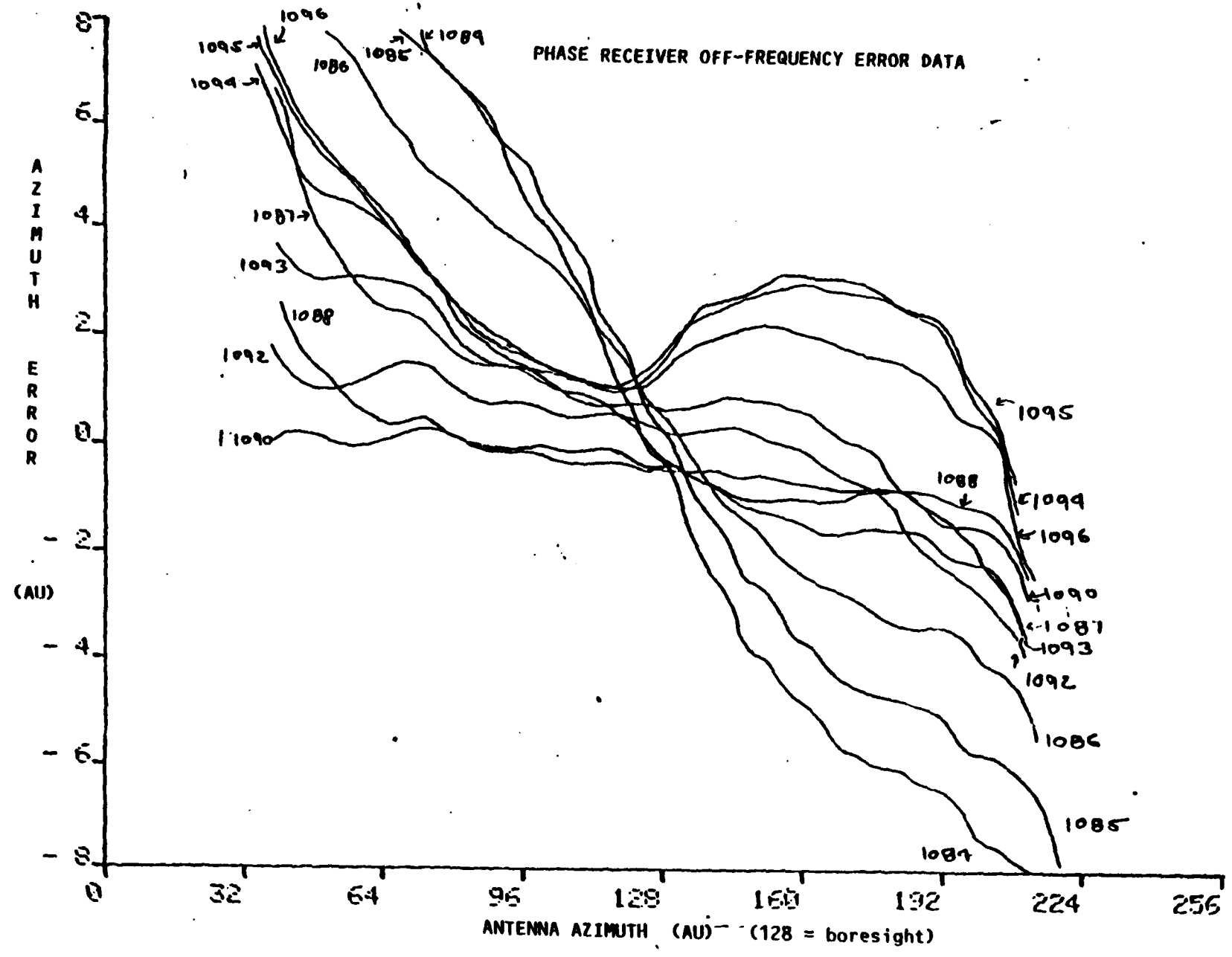
PHASE RECEIVER OFF-FREQUENCY ERROR DATA
AZIMUTH ERROR (AU)
8
6
4
2
0
-2
-4
-6
-8
0
32
64
96
128
160
192
224
256
ANTENNA AZIMUTH (AU) (128 = boresight)
1096
1095
1089
1086
1085
1094
1087
1093
1088
1092
1090
1095
1088
1094
1096
1090
1087
1093
1092
1086
1085
1084

FIGURE 19a

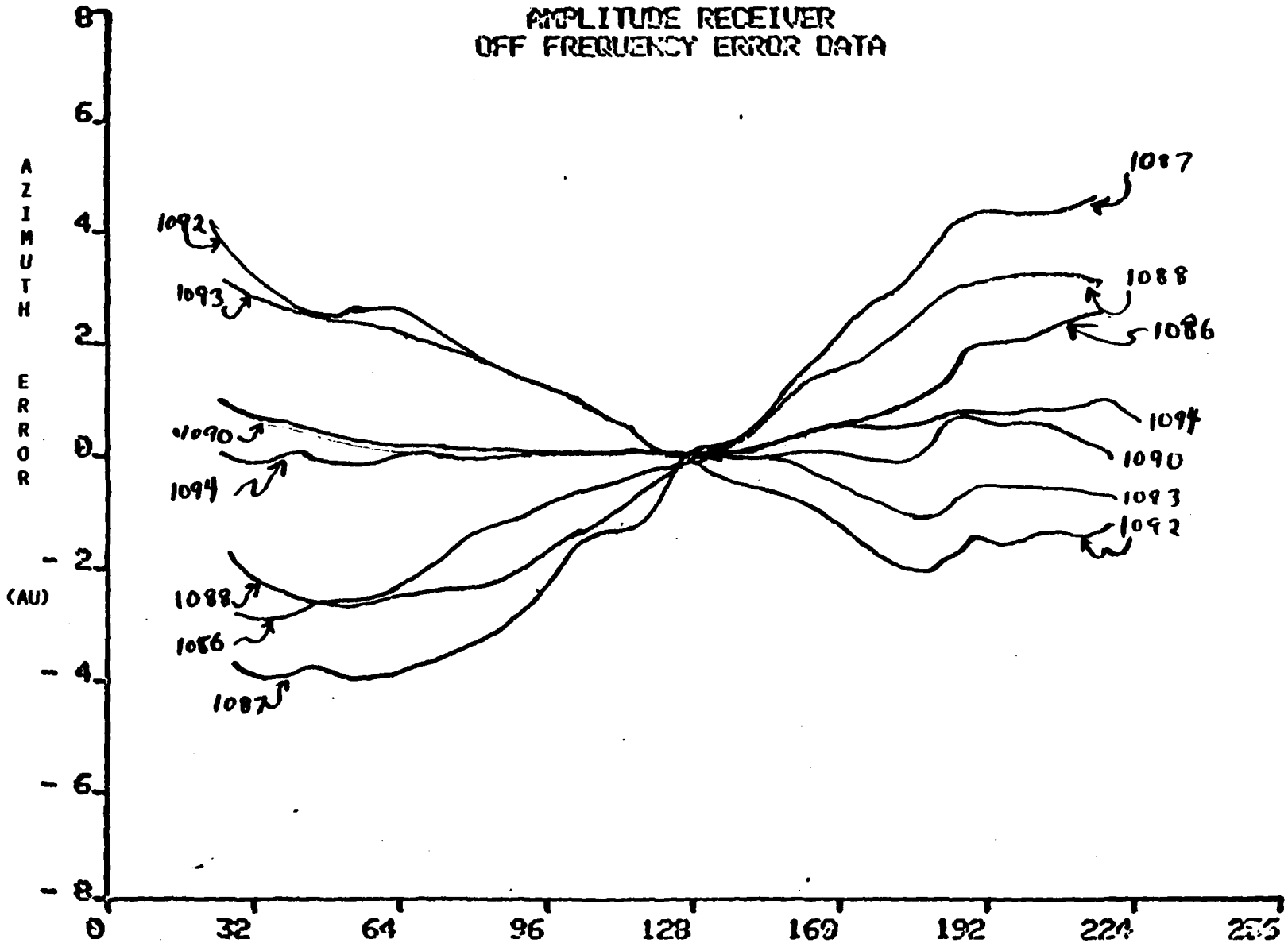
AMPLITUDE RECEIVER
OFF FREQUENCY ERROR DATA
AZIMUTH ERROR (AU)
8
6
4
2
0
-2
-4
-6
-8
0
32
64
96
128
160
192
224
256
1092
1093
1090
1094
1088
1086
1087
1087
1088
1086
1094
1090
1093
1092
ANTENNA AZIMUTH (AU) (128 = boresight)

FIGURE 19b

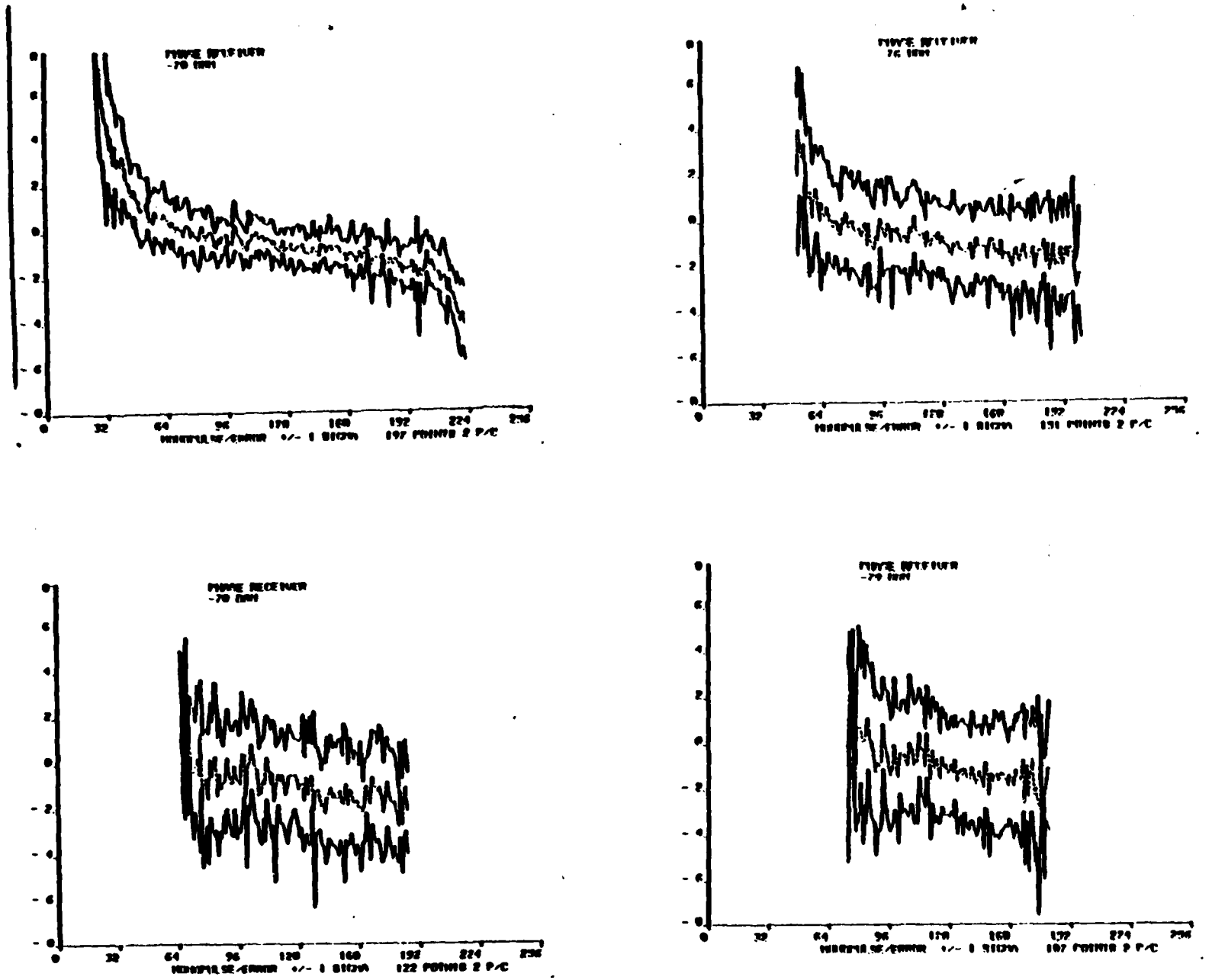

FIGURE 20. PHASE RECEIVER LOW POWER ERROR

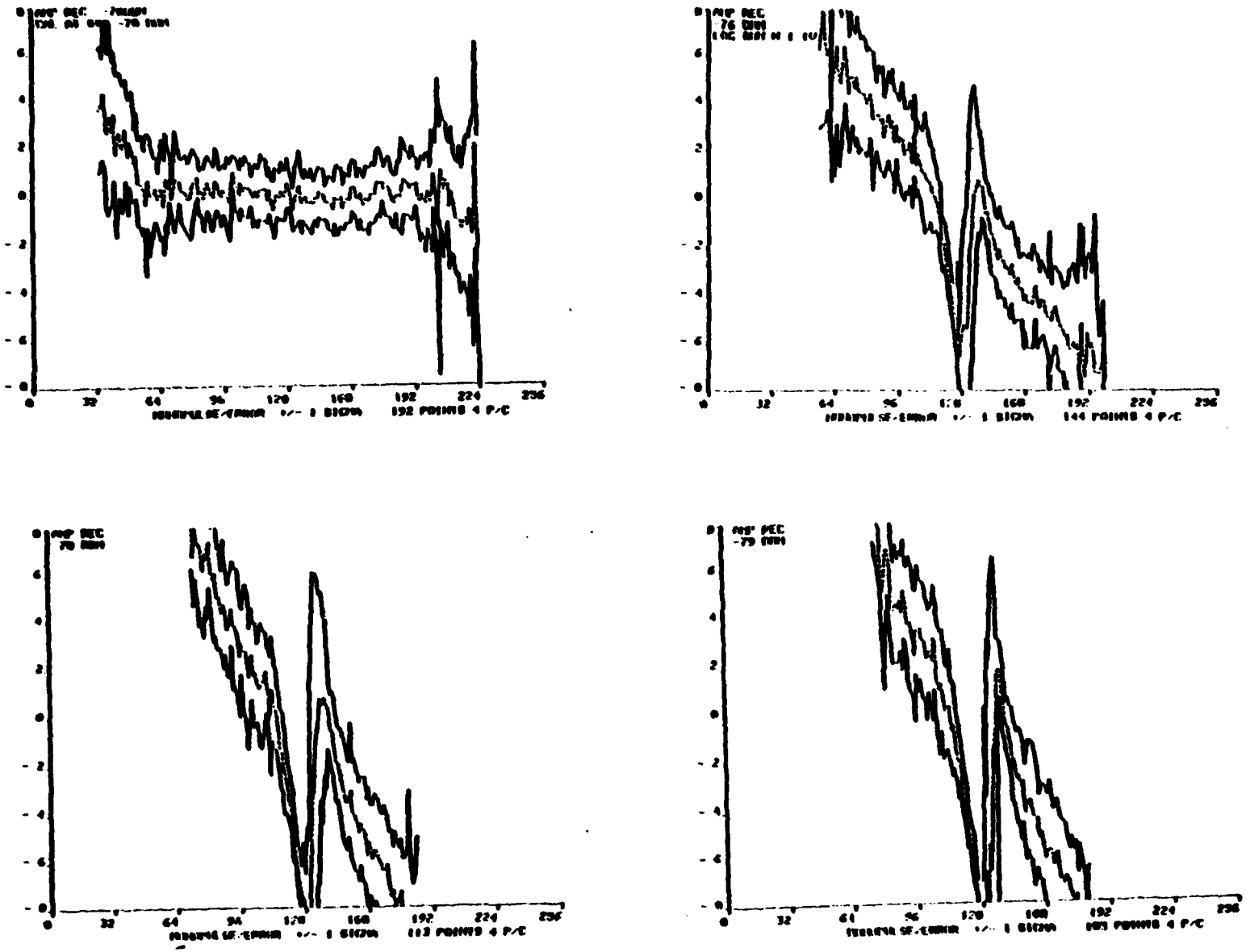

FIGURE 21. AMPLITUDE RECEIVER LOW POWER ERROR

The data for both receivers show a narrowing of the beam at reduced signal levels. This is due primarily to fixed video thresholds (TSA-Fixed Sum ATCRBS and TSD-Fixed Sum Mode S) used to eliminate low level replies. Since these thresholds were set to -82 dBm then replies below this point were rejected resulting in an apparent reduction of the beamwidth. It should be noted that at a {D}/{S} ratio of +6 dB the sum antenna pattern for the 5-foot open array is 9 dB down from the peak of the beam and occurs at approximately 1.8 degrees on either side of boresight (3.6 degrees total beamwidth).

Results of the tests performed on the amplitude receiver show a slope in the error curve as the received signal level is reduced from the -70 dBm calibration curve. The slope itself is essentially the result of the tracking limitations of the log amplifiers. Similar type slopes were noted during Power Variation testing in this effort. In the areas near boresight the {D}/{S} ratio is effectively limited to approximately -25 dB before the SNR for the {D} signal is equal to 0 dB. A second factor in this regard is that the phase detector for sensing right and left of boresight is more subject to the effects of noise with the reduction of the {D} signal. These effects are, of course, more pronounced due to the +/-1 dB tracking tolerance already identified for the logarithmic amplifiers.

The phase receiver shows an increase in the deviation of the error, not unlike that of the amplitude receiver, but the mean error tended to remain close to zero across the entire beam. The relative flatness of the mean error is, in part, due to the equal signal levels present, due to the quadrature hybrid and the ability of the components in the receiver to provide adequate phase tracking at the input to the phase detectors.

POWER VARIATIONS. The reason for these data were to present the error produced by changes in received power levels. This factor becomes critical when evaluating the amplitude receiver tested because of the +/-1 dB tracking tolerance of the log amplifiers. The tests were performed by calibrating at -54 dBm, and than collecting error data at power levels from 1 to 9 dB below that. The plot references CPME attenuator settings of 2 dB to 11 dB, where 2 dB results in receieved power of -54 dBm and each addition dB of attenuation causes 1 less dB in received power.

The amplitude receiver produced azimuth errors as shown in figure 22. This error is due primarily to the log amplifier tracking problem and their approximated log curve output.

The same tests were run on the phase receiver with no noticable effect. Therefore, no plots are presented.

FLIGHT TESTS

The flight test data for both the phase and amplitude receivers were filtered with respect to elevation in order to minimize the bias effects that occur with increasing elevation angles (reference 3). The range of filtering was from 0 to 10 and from 10 to 20 degrees elevation for both transponder types (Mode S and ATCRBS).

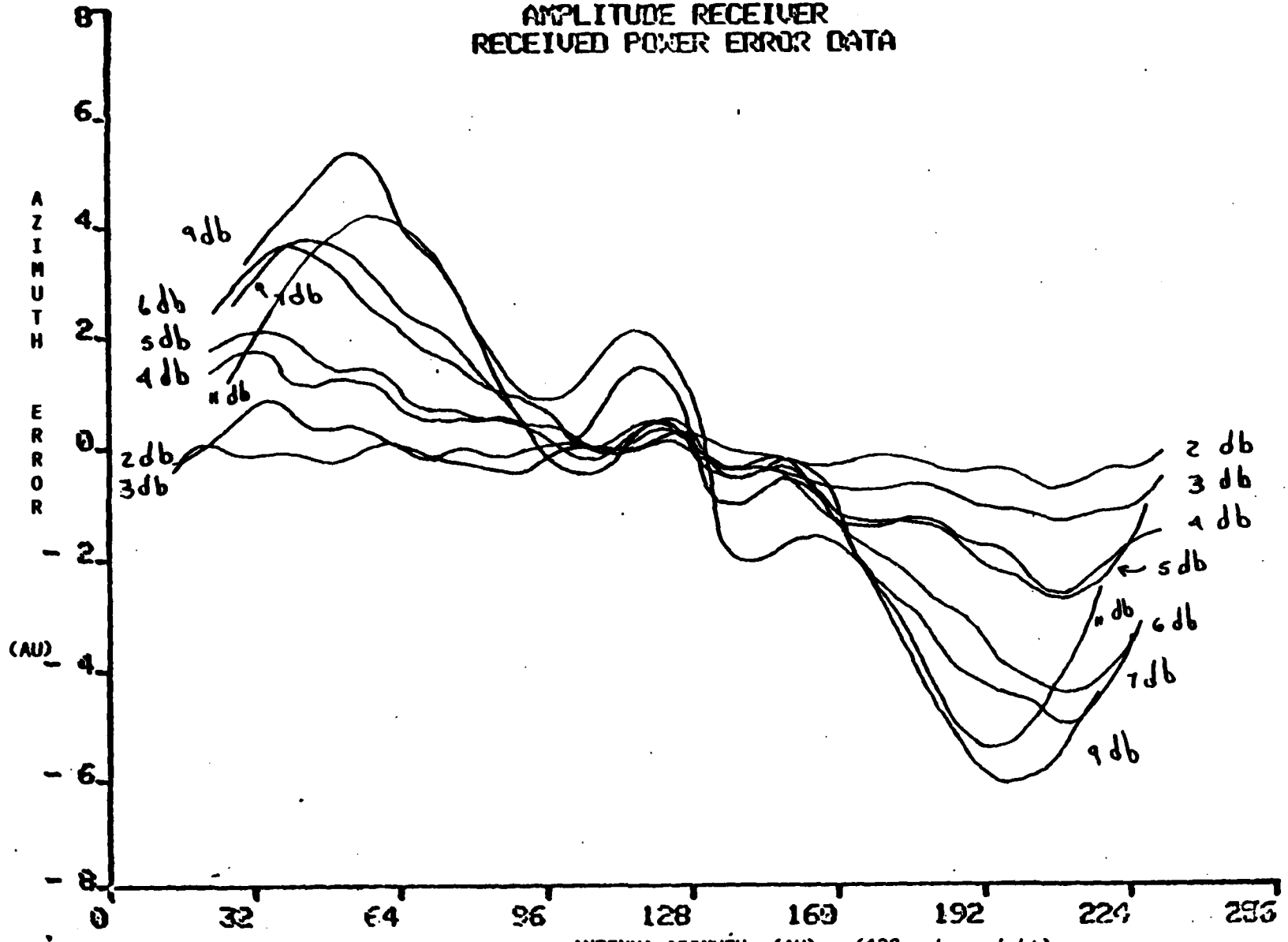
AMPLITUDE RECEIVER
RECEIVED POWER ERROR DATA
AZIMUTH ERROR
(AU)
8
6
4
2
0
-2
-4
-6
-8
0
32
64
96
128
160
192
224
256
9db
7db
6db
5db
4db
2db
3db
2 db
3 db
4 db
5db
6db
7db
9db
ANTENNA AZIMUTH (AU) (128 = boresight)

FIGURE 22

The mean and standard deviation of the flight results are compared in table 4. The results of the phase receiver were comparable to those derived during prior system accuracy tests performed on the Mode S sensor at the Technical Center (reference 3). Figure 23A shows a mean error for Mode S replies of 2 a.u.'s below 10 degrees and 1 AU's for 10 to 20 degrees. The one sigma deviation is similar for both. The ATCRBS results had smaller mean and one sigma stantard devaitions due, primarily, to the fact that the replies used for ATCRBS processing are close to boresight, while Mode S are taken at the beam edge. Figure 23B presents this data.

The amplitude data presented in figures 24A and 24B show a much larger mean and standard deviation for both ATCRBS and Mode S. This is due primarily to the 15 to 20 dB variation in the received power level as the aircraft traveled from 5 to 40 miles. The ATCRBS once again had better results because the replies used to form target reports are close to boresight. The mean error for the Mode S reports below 10 degrees is 12 AU's. This is more than the 6 AU error found during the power variation test, but these tests were conducted from -54 to -63 dBm.

The flight power levels were above -50 dBm and resulted in different log amplifier tracking errors. The amount of power variation experienced and the different range of operation of the log amplifiers could account for the increased error.

INTERFERENCE TESTS

Since the effects of interference were negligible at an SNR of 40 dB, the subsequent tests were conducted with the lowest SNR at which the sensor would calibrate, 25 dB. The received CPME power at this SNR was -70 dBm.

The effects of Mode S fruit at a rate of 100/sec, at SIR's of -10, 0, and +10 dB for the two receivers were negligible. Figures 25A and B show the mean and S.D. of the azimuth error for the two receivers with no interference injected. The worst case instances for 100 Mode-S/sec, SIR equal to -10 dB injected at crossover, are shown in the error plots of figures 25C and D.

For ATCRBS fruit rates of 5K and 16K, at the SIR's tested, the mean azimuth error remained uneffected for both systems. The standard deviation became slightly erratic, some points as much as 8 AU's, at the left edge of the beam using the amplitude system under 16K ATCRBS. The results for 5K and 16K ATCRBS are shown in figure 26 for the two receivers.

The results of figures 27A and B, using 16K ATCRBS at an SIR of -20 dB, also show deviations at the edge of the beam for the amplitude system which reflect another phenomena, that is, in these areas, the number of data points used to derive the mean error and standard deviation drop off with an increasing rate of interference. This occurs, because, the data collected were filtered by the Mode S/ATCRBS processors producing only good replies. This filtering technique attempts to correlate on a pulse-by-pulse basis for ATCRBS replies, and on a chip-by-chip basis for Mode-S replies, the monopulse values of each pulse (or chip) with a monopulse estimate. The slight deviations seen at the beam edges of the error plots are the effects of interference on those replies whoses pulses have correlated only. Replies whose pulses do not correlate are rejected.

TABLE 4

FLIGHT TEST RESULTS

AZIMUTH ERRORS – MEAN & STANDARD DEVIATION (A.U.'s)

Elevation	MODE-S				ATCRBS			
	Phase		Amplitude		Phase		Amplitude	
	m	sd	m	sd	m	sd	m	sd
< 10 deg	2.1	2.7	11.1	3.5	0.1	1.4	3.8	3.8
10 – 20 deg	1.3	1.7	7.4	2.8	0.5	1.0	4.4	2.8

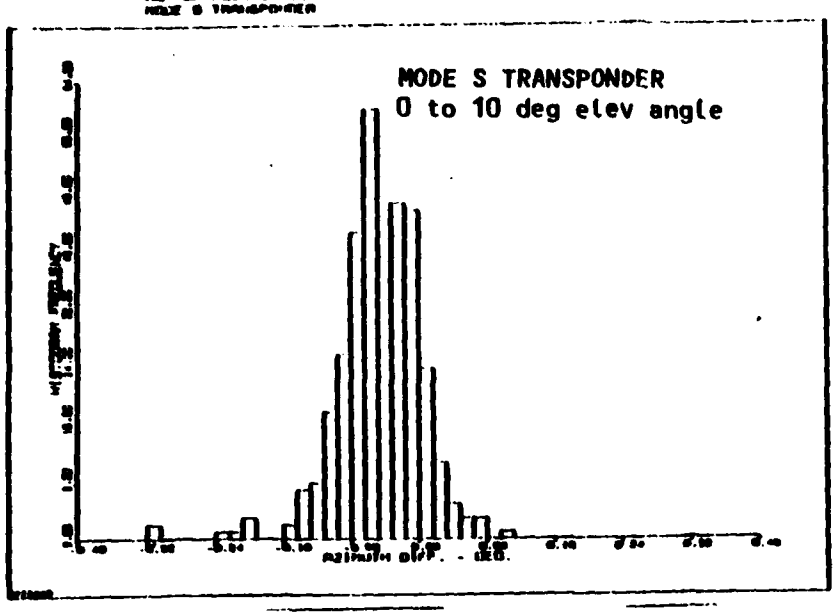

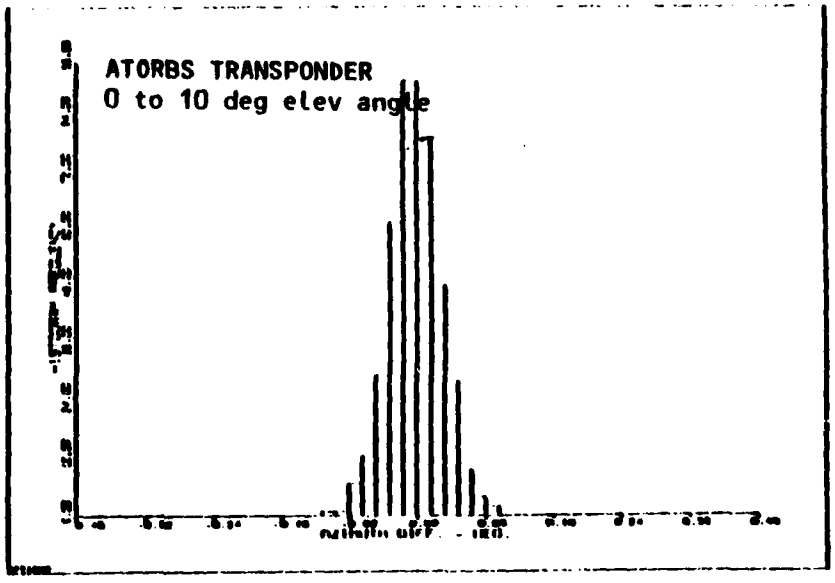

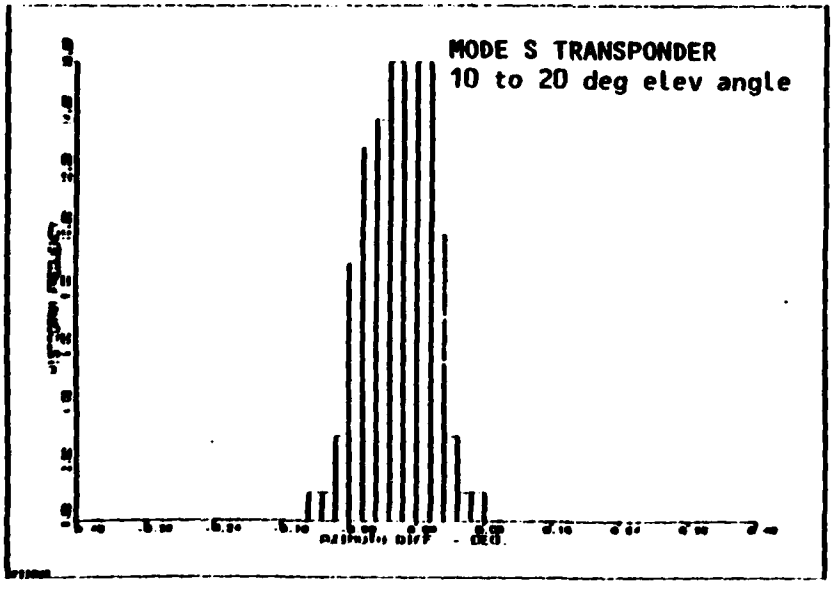

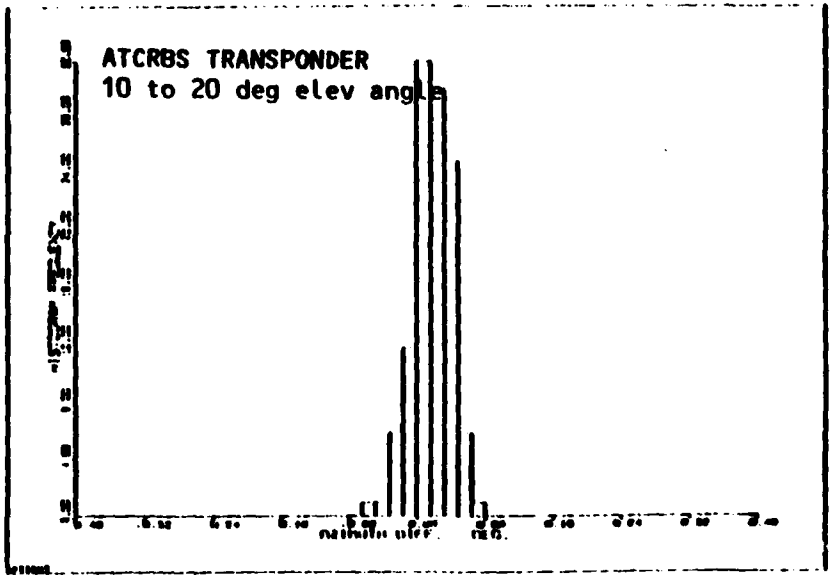

PHASE RECEIVER FLIGHT TEST AZIMUTH RESIDUAL HISTOGRAMS
FIGURE 23

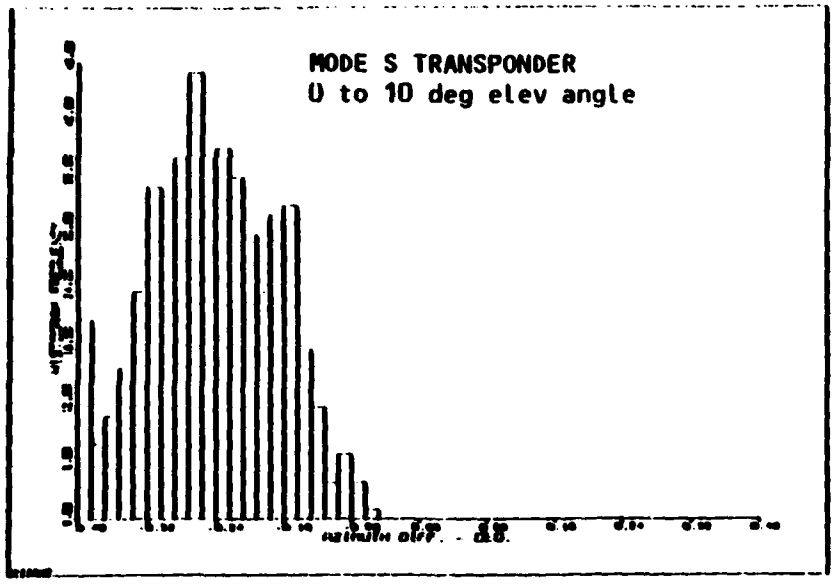

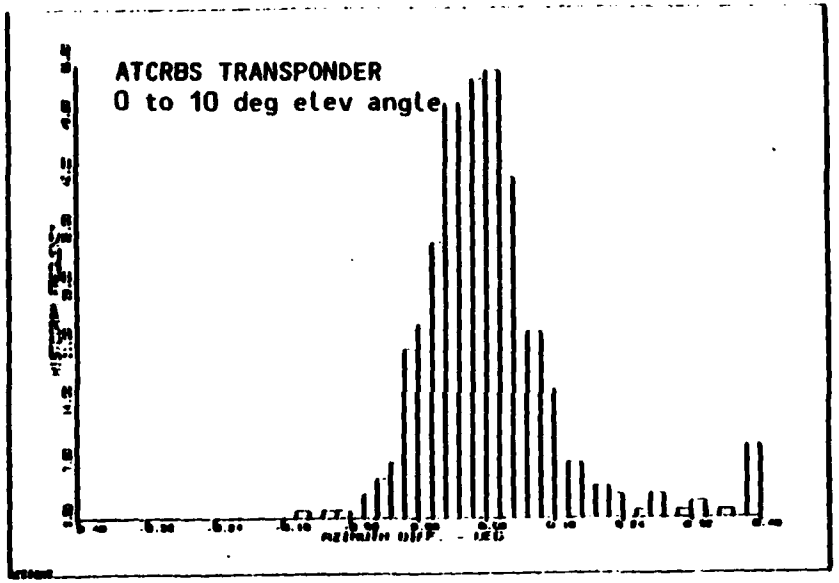

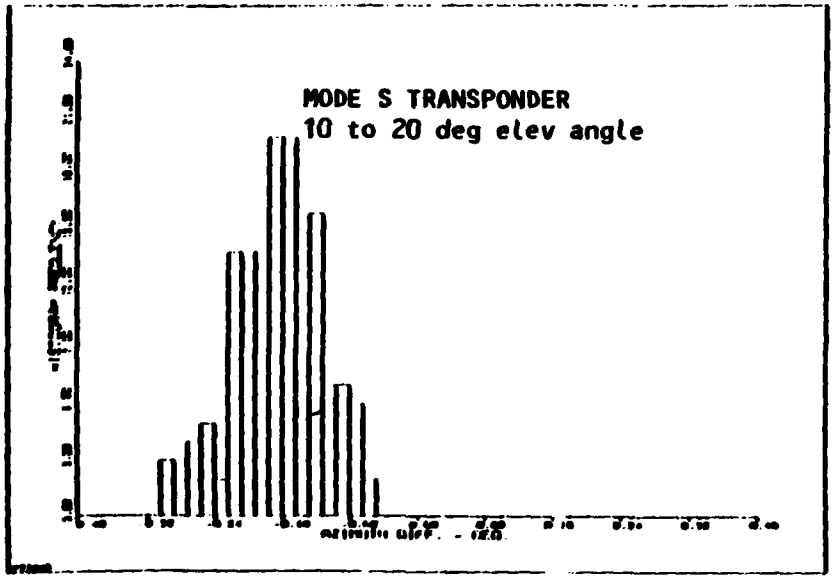

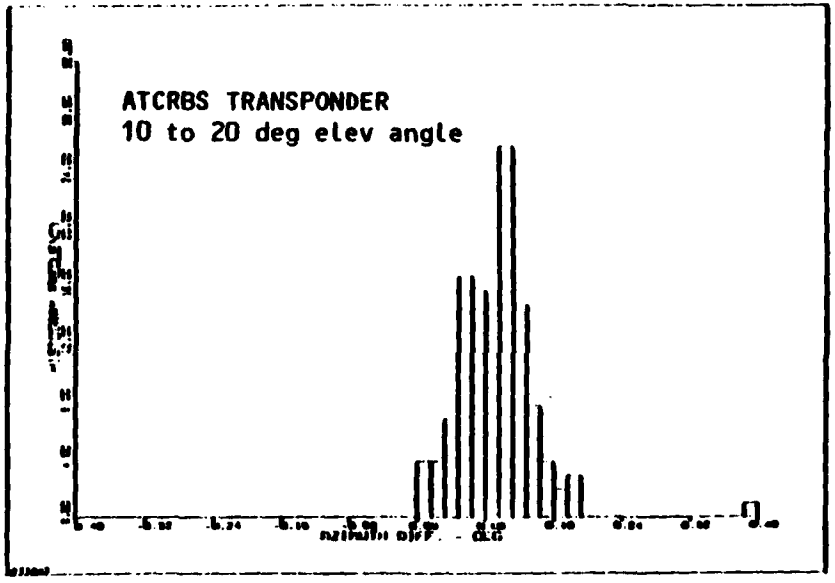

AMPLITUDE RECEIVER FLIGHT TEST AZIMUTH RESIDUAL HISTOGRAMS
FIGURE 24

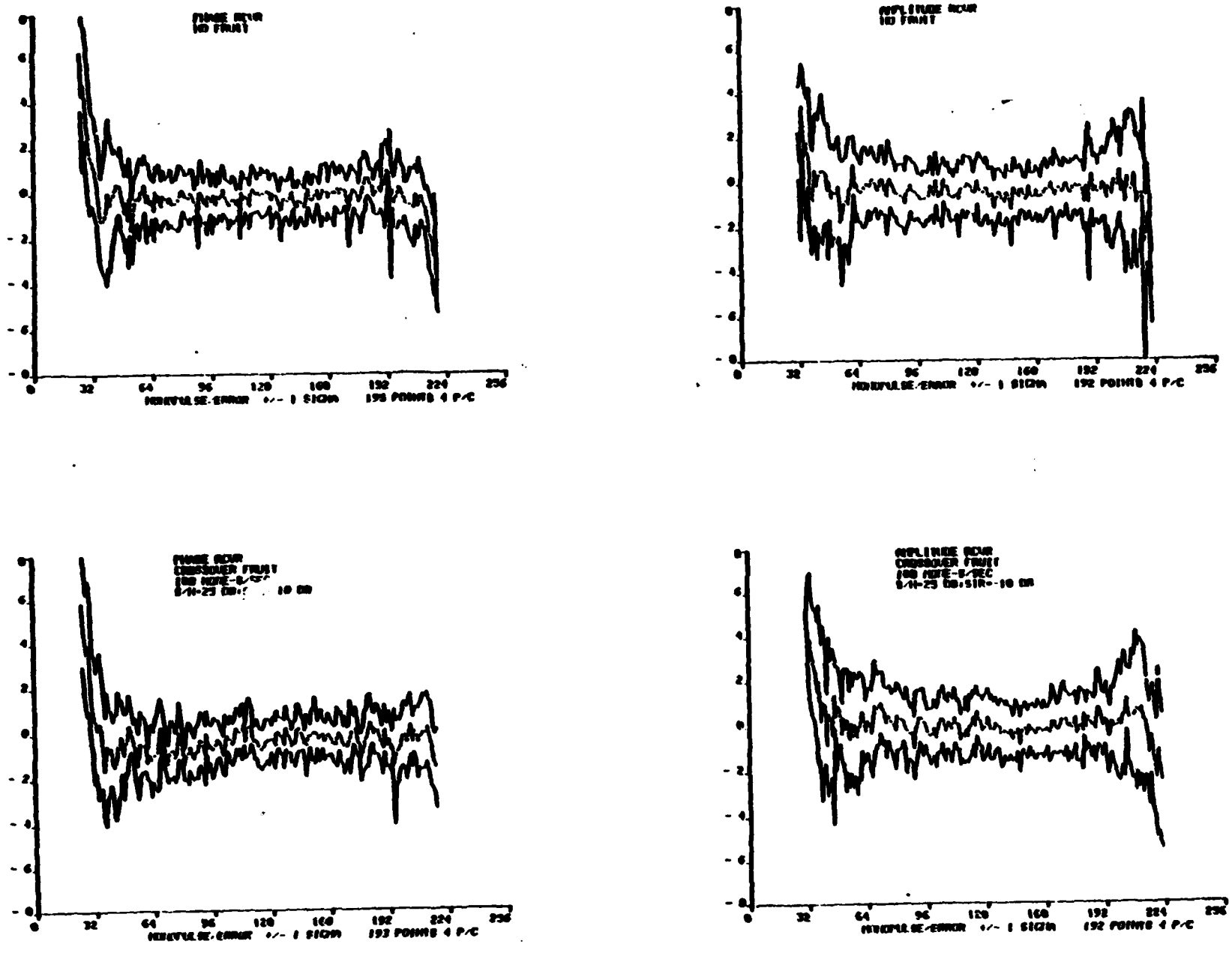

FIGURE. 25 INTERFERENCE EFFECTS

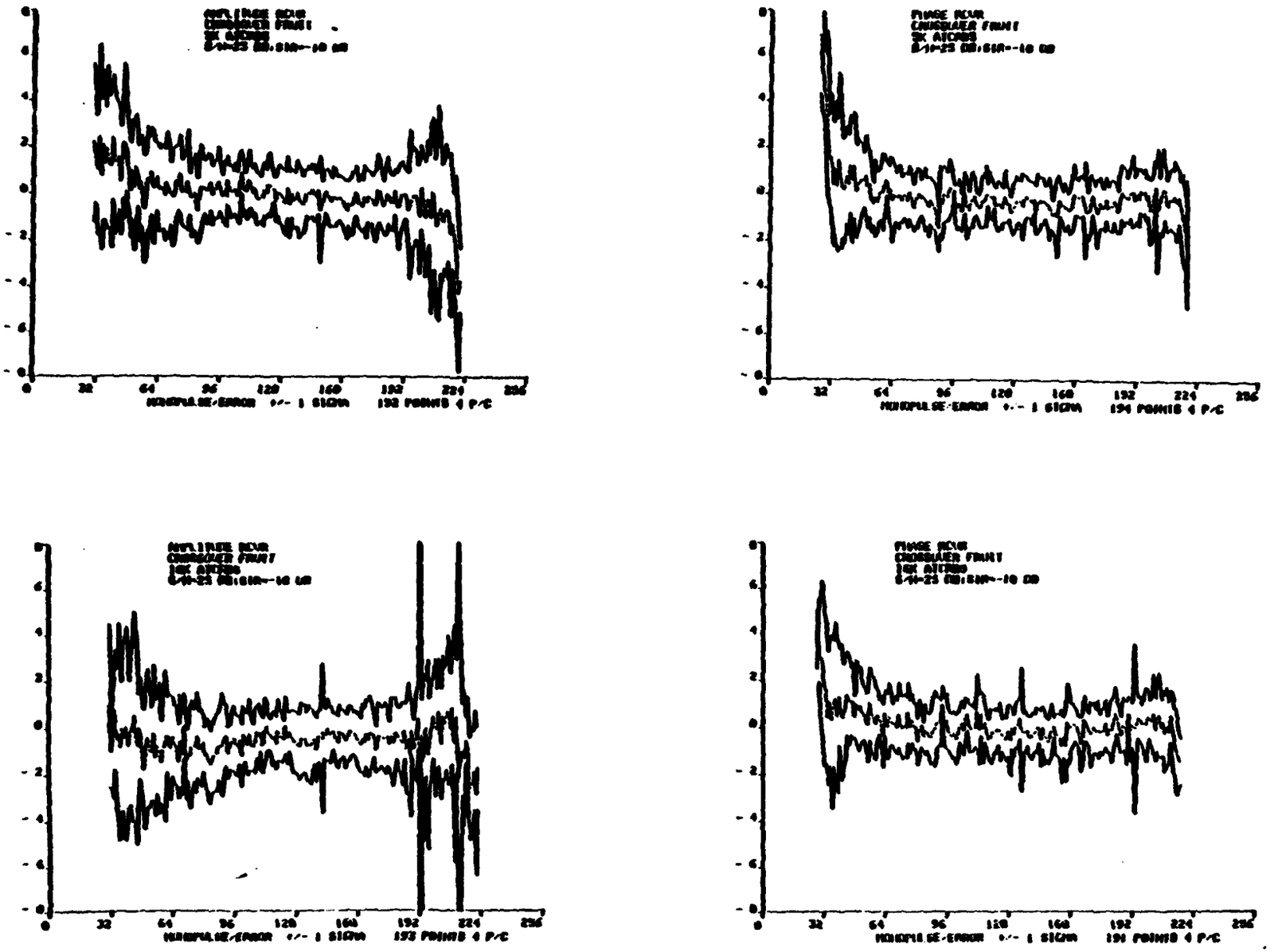

FIGURE. 26 INTERFERENCE EFFECTS

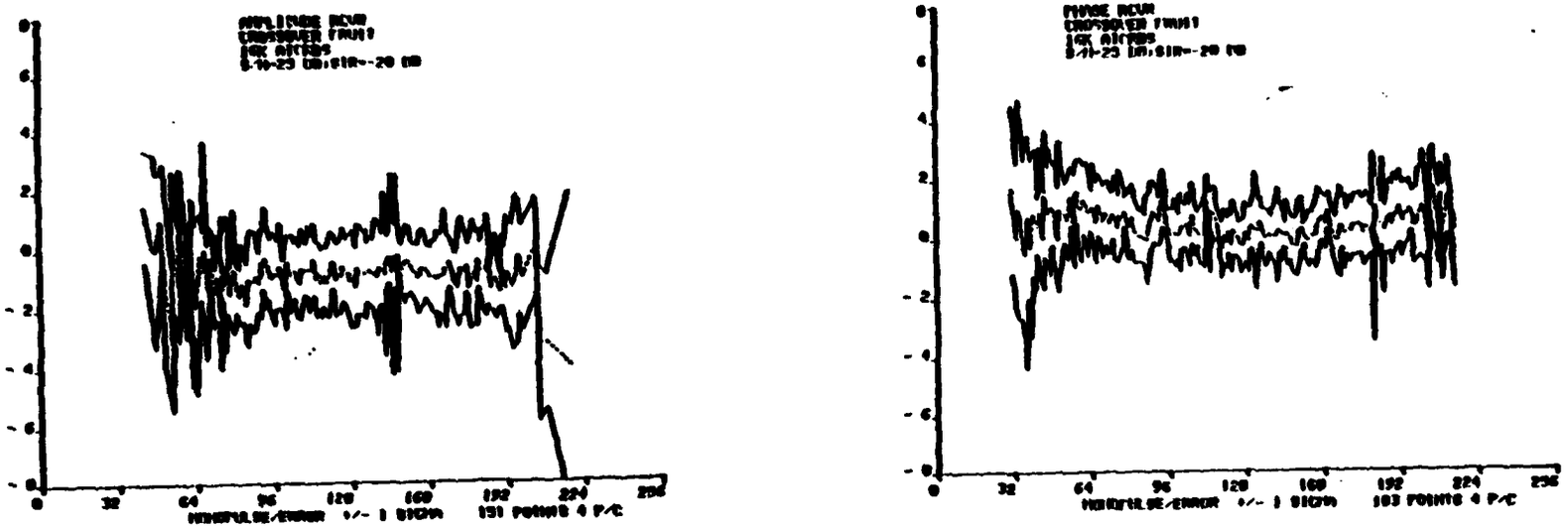

FIGURE. 27 INTERFERENCE EFFECTS

The number of replies accepted by the Mode S/ATCRBS processors and, therefore used to form the plots mentioned above are tabulated for each receiver in table 5. The interference conditions are the same as those used in forming the above plots: crossover injected fruit at rates of 100 Mode S, 5K, and 16K ATCRBS, at SIR's of -10 and -20 dBm. The number of accepted replies under Mode S interference remained equal to the amount under no inteference for both receiver types. The number of replies did not decrease appreciably until an interference rate of 16K and an SIR of -20 dB was used, the amplitude receiver suffering the most effects, although this table is more an indication of how well the Mode S/ATCRBS processors are functioning in conjunction with each of the receivers than the relative merits of either the phase or amplitude receiver alone.

TABLE 5

MODE-S REPLIES/SCAN UNDER INTERFERENCE

Fruit	# of replies/scan	
	Amplitude Rcvr	Phase Rcvr
None	135	135
100 Mode-S/sec (SIR=-10 DB)	135	135
1.5 K ATCRBS "	135	135
5 K ATCRBS "	130	133
16 K ATCRBS "	125	127
16 K ATCRBS (SIR=-20 dB)	70	112

SUMMARY OF RESULTS

The salient features of the results presented in the foregoing section are presented here to provide a relative comparison of the two receiver designs.

1. Linearity of Monopulse Output:
   From the results of the static tests the phase receiver has a marked edge in terms of the consistency of the {D}/{S} output with changes in input power. The prime limitation of the amplitude lay in the relative tracking of the logarithmic amplifiers and the already +/-1 dB db ripple that results for the {D}/{S} ouput. The phase receiver shows little if any affect with variations in input power.

2. Dynamic Range:
   The overall dynamic range of each receiver, at least for detection purposes, was comparable (less than -80 dBm for 90 percent detection).

3. Frequency Effects:
   Results of frequency varitaions for both receivers tended to favor the amplitude receiver with a smaller maximum error of +/- 4 AU's over a wider bandwidth (1090+/-4 MHz) when compared with that of the phase receiver over the same frequencies (+/- 8 AU's).

4. Low Signal Level Operation:
   Operation of each receiver at low received signal levels, i.e, 79 dBm favors the phase receiver in terms of a negligible mean error when compared to the amplitude receiver over the effective beamwidth. In both receivers the effective beamwidth was reduced due to fixed video thresholds used in the sensor to limit low level replies. The mean error curve for the amplitude receiver possessed a slope with a maximum error of 8 AU's at the ends of the effective beam. In both receivers the variance of the errors increased at reduced signal levels. The amplitude receiver was also affected near boresight due to the {D} signal being at or below the receiver's noise level.

5. Accuracy Flight Results:
   Accuracy during the flight tests revealed increased bias errors for the amplitude receiver when compared with the phase receiver. For both ATCRBS and Mode S replies, the phase receiver demonstrated bias errors of less than 2 AU's. The amplitudde receiver, however, gave target reports with azimuth errors of as much as 5 AU's for ATCRBS replies and 12 AU's for Mode S replies.

6. Susceptibility to Interference:
   Both phase and amplitude receivers suffer no ill effects under a Mode S interference rate of 100 per second or an ATCRBS inteference rate of 1.7K per second. The amplitude receiver begins to show a slight increase in error at the edge of the beam under 5K and 16K ATCRBS interference rates. For both receivers the number of detected replies decreases as the inteference rate increases from 16K or the SIR decreases from -10 dB, with the phase receiver's performance slightly better.

CONCLUSION

Based on the overall results of the tests described in this report, the phase receiver provided better azimuth accuracy results than did the amplitude receiver. It was noted however, that the accuracy of the amplitude receiver used in this effort was limited in part by the +/-1 dB ripple that existed between the (S) and (D) logarithmic amplifiers.

During the tests both receivers were operated over a beamwidth in excess of 4.5 degrees with only one limitation noted. Namely, the off-frequency results for the phase receiver tended to increase beyond 8 AU's at the beam edge for certain frequencies in the band from 1086 to 1094 MHz. This characteristic has already been identified for the phase receiver in reference 10.

The amplitude receiver demonstrated some frequency sensitivity over the 1090 +/-4 MHz range tested. The errors induced by this sensitivity tende to have a smaller maximum value than in the phase receiver. The errors also tended to be more linear with respect to the (D)/(S) ratio than did the phase receiver.

The results of the flight tests tended to be consistent with other results derived during this effort. Namely, the amplitude receiver had an accuracy limitation that can be attributed to the relative tracking of the log amplifiers. Accuracy for ATCRBS replies was somewhat better than for the Mode S replies primarily due to the weighting that the interrogation algorithm gave for ATCRBS replies near boresight while Mode S target reports were based on replies at the forward edge of the beam. The phase receiver gave better accuracy than the amplitude receiver for both ATCRBS and Mode-S replies.

Interference effects on the azimuth accuracy of Mode S replies were only marginally different from the no interference case for the amplitude receiver. The effects were limited to occasional spikes of 8 AU's in the azimuth bias. Similar excursions were not noted for the phase receiver. A secondary effect was found to be at work in both receivers when the SIR was decreased to -20 dB while the ATCRBS fruit rate was maintained at 16K/sec. The effect was manifest by a reduction in the number of replies received and correctly decoded by the sensor's Mode S processor. In this case the phase receiver showed the impact of the interference only slightly less than the amplitude receiver.

Both receivers remained unaffected by Mode S interference rates of 100/sec at SIR's between -20 and +10 dB.

REFERENCES

1. Federal Aviation Administration, "Discrete Address Beacon System - Phase II," Engineering Requirement, FAA-ER-240-26, November 1, 1974.

2. Karp, D., Wood, M. L., "DABS Monopulse Summary," Lincoln Laboratory, MIT Report ATAC-72, FAA-RD-76-219, February 4, 1977.

3. Chapman, C., Brady, J., "Mode S System Accuracy," Final Report, DOT/FAA/RD-81/90, February 1982.

4 Kenton, John, "Comparison of Phase and Amplitude Monopulse Receivers" Letter Report, CT-82-100-10LR, December 1981.

5. Kenton, John, "Interference Tests on Phase and Amplitude Monopulse Receivers," Addendum to Letter Report, CT-82-100-LR10, January 1982

6. Greenberg, M., "Summary of Transponder Data May 1979 through Novenber 1979," Data Report, FAA-CT-81-5, Currently Unpublished.

7. Greenberg, M., "Summary of Transponder Data June 1977 through August 1978," Interim Report, FAA-RD-79-56, August 1979.

8. Greenberg, M., "Summary of Transponder Data for Atlanta, Georgia Area," Final Report, FAA-CT-80-39, October 1980.

9. Livings, J., "Modifications to the RAA Diagnostic Program of the Mode S Sensor," Letter Report, CT-82-100-31LR, February 1982.

10 Alimenti, R. J., Fox, D. P., "DABS Open Array Frequency Sensitivity Error Measurements," Letter Report, CT-81-100-5-LR, June 1981.

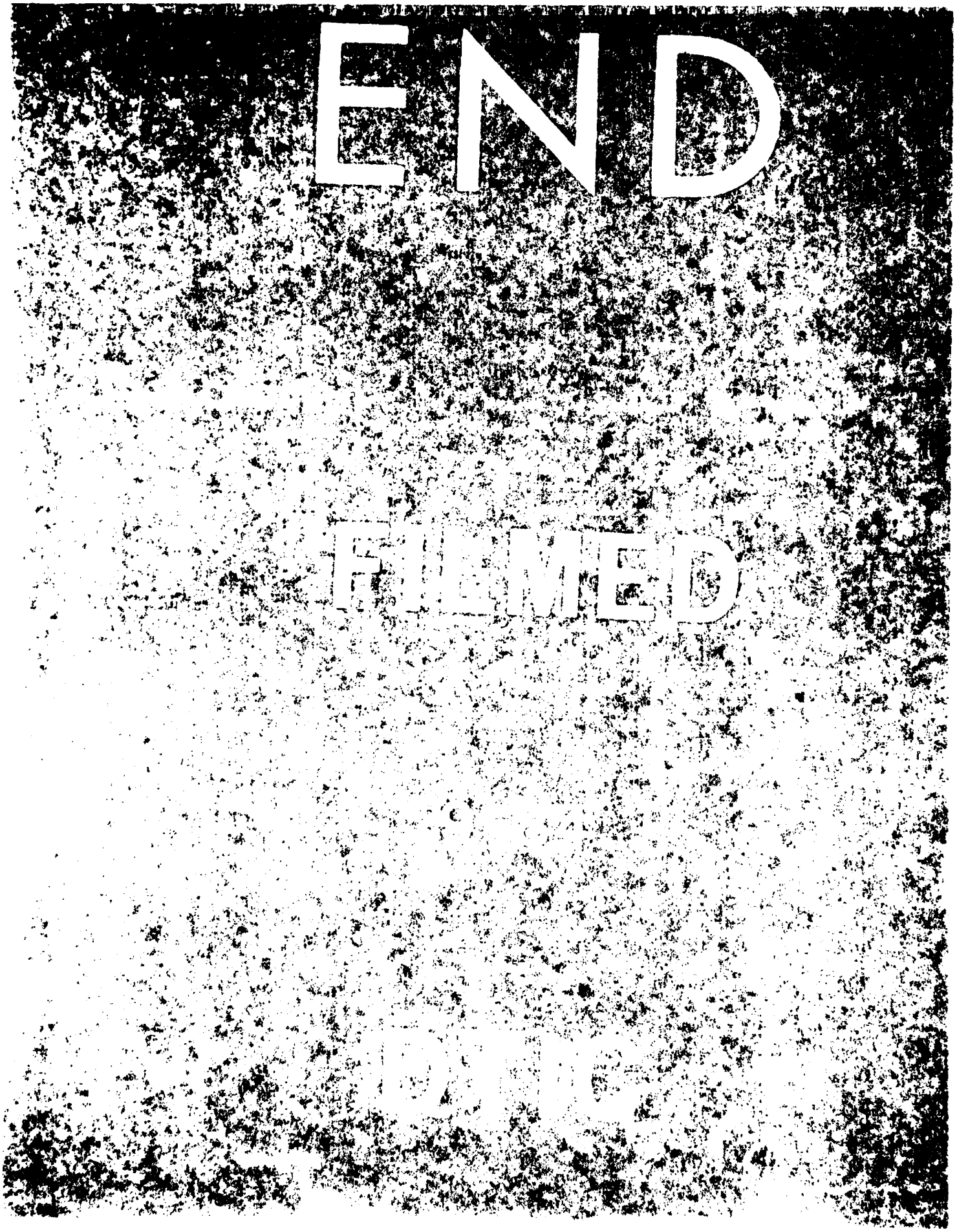
END
FILMED